

This manuscript has been submitted for publication in **ESTUARINE, COASTAL AND SHELF SCIENCE**. Please note that, despite having undergone peer review, the manuscript has yet to be formally accepted for publication. Subsequent versions of this manuscript may have slightly different content. If accepted, the final version of this manuscript will be available via the '***Peer-reviewed Publication DOI***' link on the right-hand side of this webpage. Please feel free to contact any of the authors; we welcome feedback.

Estuarine, Coastal and Shelf Science

Laboratory and field investigations to characterize the resistivity and induced polarization response of heterogeneous coastal aquifers

--Manuscript Draft--

Manuscript Number:	
Article Type:	Research Paper
Keywords:	aquifer, saltwater intrusion, conductivity, resistivity, induced polarization
Corresponding Author:	Diep Cong-Thi, Ph.D student Ghent University BELGIUM
First Author:	Diep Cong-Thi, Ph.D student
Order of Authors:	Diep Cong-Thi, Ph.D student Linh Pham Dieu David Caterina Xavier De Pauw Huyen Dang Thi Hieu Huu Ho Frédéric Nguyen Thomas Hermans
Abstract:	<p>The lithological and stratigraphical heterogeneity of coastal aquifers has a great influence on saltwater intrusion (SI). This makes it difficult to predict SI pathways and their persistence in time. In this context, electrical resistivity tomography (ERT) and induced polarization (IP) methods are receiving increasing attention regarding the discrimination between saltwater-bearing and clayey sediments. To simplify the interpretation of ERT data, it is commonly assumed that the bulk conductivity mostly depends on the conductivity of pore-filling fluids, while surface conductivity is generally disregarded in the spatial and temporal variability of the aquifers, particularly, once the aquifer is affected by the presence of saltwater. Quantifying salinities based on a simplified petrophysical relationship can lead to misinterpretation of aquifers constituted by clay-rich sediments. In this study, we rely on co-located data from drilled boreholes to formulate petrophysical relationships between bulk and fluid conductivity for clay-bearing and clay-free sediments. We investigate both the laboratory scale through spectral induced polarization (SIP) and field-scale through the comparison of ERT and time-domain IP with electromagnetic logging and lithologs. First, the sedimentary samples from the drilled wells were classified according to their particle size distribution and then analyzed in the lab using a SIP system using the four-point measurement method in controlled salinity conditions. Second, field inversion results were compared with logging results and direct salinity measurements on water samples. We find that the formation factors and surface conductivity of the different unconsolidated sedimentary classifications are varying from 4.0 to 8.9 for coarse-grained sand and clay-bearing mixtures, respectively. The clay-bearing sediments are mostly distributed in discontinuous small lenses along the Luy River Catchment. The assumption of homogenous geological media is therefore leading to overestimating SI in the heterogeneous clay-bearing aquifers.</p>
Suggested Reviewers:	Damien Jougnot damien.jougnot@upmc.fr Adrian Flores-Orozco adrian.flores-orozco@geo.tuwien.ac.at Lee Slater lslater@newark.rutgers.edu Mike Mueller-Petke

	mike.mueller-petke@leibniz-liag.de
--	------------------------------------

Opposed Reviewers:	
---------------------------	--

Laboratory and field investigations to characterize the resistivity and induced polarization response of heterogeneous coastal aquifers

D. Cong-Thi^{1,2}, L. Pham Dieu^{1,2}, D. Caterina³, X. De Pauw¹, H. Dang Thi², HH. Ho², F. Nguyen^{3,4}, T. Hermans¹

(1) Department of Geology, Ghent University, 9000-Gent, Belgium.

(2) Department of Marine Geology, Vietnam Institute of Geosciences and Mineral Resources (VIGMR), 100000 Hanoi, Vietnam.

(3) Department of Urban and Environmental Engineering, Liege University, B52- 4000 Liège, Belgium.

(4) Department of Civil Engineering, KU Leuven, 3000 Leuven, Belgium.

Corresponding author: diep.congthi@ugent.be, Thomas.Hermans@ugent.be

Abstract. The lithological and stratigraphical heterogeneity of coastal aquifers has a great influence on saltwater intrusion (SI). This makes it difficult to predict SI pathways and their persistence in time. In this context, electrical resistivity tomography (ERT) and induced polarization (IP) methods are receiving increasing attention regarding the discrimination between saltwater-bearing and clayey sediments. To simplify the interpretation of ERT data, it is commonly assumed that the bulk conductivity mostly depends on the conductivity of pore-filling fluids, while surface conductivity is generally disregarded in the spatial and temporal variability of the aquifers, particularly, once the aquifer is affected by the presence of saltwater. Quantifying salinities based on a simplified petrophysical relationship can lead to misinterpretation of aquifers constituted by clay-rich sediments. In this study, we rely on co-located data from drilled boreholes to formulate petrophysical relationships between bulk and fluid conductivity for clay-bearing and clay-free sediments. We investigate both the laboratory scale through spectral induced polarization (SIP) and field-scale through the comparison of ERT and time-domain IP with electromagnetic logging and lithologs. First, the sedimentary samples from the drilled wells were classified according to their particle size distribution and then analyzed in the lab using a SIP system using the four-point

26 measurement method in controlled salinity conditions. Second, field inversion results were
27 compared with logging results and direct salinity measurements on water samples. We find that
28 the formation factors and surface conductivity of the different unconsolidated sedimentary
29 classifications are varying from 4.0 to 8.9 for coarse-grained sand and clay-bearing mixtures,
30 respectively. The clay-bearing sediments are mostly distributed in discontinuous small lenses
31 along the Luy River Catchment. The assumption of homogenous geological media is therefore
32 leading to overestimating SI in the heterogeneous clay-bearing aquifers.

33 Keywords: aquifer, saltwater intrusion, conductivity, resistivity, induced polarization.

35 1. Introduction

36 Saltwater intrusion (SI) in coastal aquifers is one of the serious problems that numerous
37 countries have to face, particularly countries with long coastlines. It has not only a significant local
38 influence through the degradation of water resources, but it affects the general development of a
39 country (Insigne and Kim, 2010; Post et al., 2018).

40 If SI can be dominated by anthropogenic activities including the overexploitation or
41 uncontrolled use of groundwater resources, natural causes related to the structure, shape, and
42 lithological constituents of aquifers combined with the past climatic, geological and tectonic
43 context must also be considered (Cong-Thi et al., 2021a; Dieu et al., 2022). In conditions of rising
44 sea-level, the deposition of fine-grained sediments is dominant, resulting in forming clay-rich
45 sedimentary strata. Inversely, in the case of decreasing sea level, the previously deposited
46 formations are altered and eroded. Alluvial, aeolian, and lacustrine sedimentation, depending on
47 the flow conditions, dominate leading to sedimentary sequences with a broad range of grain sizes
48 (Krumbein, 1934; Krumbein and Sloss, 1963). The succession of numerous regression-
49 transgression cycles is the main cause for the formation of complex depositional sequences,
50 resulting in the strong heterogeneity of many coastal aquifers (Koster and Sulter, 1993; Miall,
51 2000; Ta et al., 2001; Thanh et al., 2017).

52 From a hydrogeological perspective, mapping the geometry and physical properties of
53 aquifers in a coastal setting is a difficult task and requires a large amount of data. Frequently, this
54 task relies on previously collected geological information pertaining to lithological and
55 stratigraphic records, but it is time-consuming and lacks reliability when the data are too sparse.
56 To generate continuous and spatially distributed data, borehole logs can be combined with
57 geophysical methods (Martínez et al., 2009; Baines et al., 2022).

58 Electrical Resistivity Tomography (ERT) is sensitive to the resistivity variations of the
59 subsurface which depends on the pore-filling fluid and lithology. Recovering the lithological
60 heterogeneity of coastal aquifers from ERT is a peculiarly critical task, particularly in saline
61 conditions (Nguyen et al., 2009; Tassy et al., 2019). To estimate the salinity from the bulk
62 resistivity distribution, a petrophysical relationship must be used. Archie's law (Archie, 1942) is
63 still the most commonly used approach. It calculates the formation factor (F) which is the ratio
64 between the conductivity of pore fluids and that of the porous medium, making it representative
65 of the pore-filling fluid only. The role of surface conductivity related to the electrical double layer
66 (EDL) is often ignored. However, the latter contributes significantly to the increased conductivity
67 in the presence of clay (Waxman and Smits, 1968; Vinegar and Waxman, 1984; Revil and Skold,
68 2011; Revil et al., 2017). Although the pore fluid effect is dominant in high salinity environments,
69 allowing to map saline zones with relative certainty, the surface conductivity effect prevents the
70 identification of freshwater resources when clay is present, as they can be easily misinterpreted as
71 brackish zone (Szalai et al., 2009; Michael et al., 2016; Cong-Thi et al., 2021a).

72 Induced polarization (IP) measures the ability of the subsurface to store electrical charge
73 under the impact of an electric field (Marshall et al., 1959). Time-Domain IP (TDIP) surveys are
74 conducted, similarly to ERT surveys, by sending a current into the ground while measuring the
75 resulting potential difference. After shutting the current off, the potential decay in the subsurface
76 is measured in several time windows to characterize its chargeability, which is the ratio of the
77 secondary voltage (decay) over the primary voltage of the transmitted current. Dividing the

78 chargeability by the resistivity results in the normalized chargeability that might highlight zones
79 with high surface conductive properties (Magnusson et al., 2010; Slater et al., 2002) such as clay-
80 rich media. Higher normalized chargeability is expected in clay-rich sediments while coarser-
81 grained soils including sand, gravel, and grit commonly yield lower values (Alabi et al., 2010). IP
82 surveys have proven to be an effective tool for mapping the lithological layers of unconsolidated
83 sediments, in particular the presence of clay content. However, TDIP has a low signal-to-noise
84 ratio and is therefore sensitive to noise (Dahlin et al., 2002; Dahlin et al., 2012). Combined with
85 the weak signals linked to high conductivity measured in saline conditions, it makes the method
86 quite challenging to apply for SI studies (Attwa et al., 2011).

87 An additional alternating approach at the laboratory scale is spectral induced polarization
88 (SIP) measurement. It measures the complex conductivity of the subsurface at various frequencies,
89 allowing to validate field investigations based on the petrophysical relationship at the laboratory
90 scale. SIP is considered as an optimum solution to characterize the interfacial polarization at the
91 interface between materials and pore-filling fluids (Revil and Florsch 2010; Revil and Skold,
92 2011), contributing to the complex conductivity of porous materials. If the dependence of the
93 complex conductivity on the mentioned-above factors is dissected, it will help to distinguish the
94 origin of conductive anomalies (Waxman and Smits, 1968; Vinegar and Waxman, 1984; Revil and
95 Skold, 2011).

96 In a previous study, Cong-Thi et al., (2021a) qualitatively delimited the extent of saltwater
97 intrusion in the Luy River catchment using ERT. However, in the absence of co-located data, their
98 method was based on the identification of the response of clay in freshwater conditions.
99 Intermediate values of resistivity could not be unequivocally interpreted as they could correspond
100 to clay-rich or brackish water zones. The objective of this study is to expand the understanding of
101 the petrophysical relationship in this study area based on co-located data. The discrepancy of
102 resistivity values controlled by the presence of clay minerals and salinity is identified using the
103 lithological and hydrological information. Firstly, the co-located sedimentary samples are

104 classified through particle size distribution analysis (PSD). Secondly, the petrophysical
1 105 relationship for different grain-sized patterns is estimated based on spectral induced polarization
2
3 106 (SIP). Lastly, the validity of the laboratory petrophysical relationship at the field scale is assessed
4
5 107 by comparing ERT and TDIP data with high-resolution logs and total dissolved solids (TDS)
6
7
8 108 content from water samples.
9

109 **2. Study area**

110 The Luy River catchment is located in Binh Thuan, a Southern Central province in Vietnam
111 (Fig. 1), and is governed by a complex geological and tectonic context. Terrains on both sides of
112 the river are quite different: low plains dominate on the left bank, while huge sand dunes are
113 present on the opposite bank. Along the Luy River, the unconsolidated sedimentary sequences
114 formed during both the Pleistocene and Holocene periods are discontinuously present in various
115 thicknesses. The Pleistocene sediments were deposited during successively transgressive and
116 regressive stages (Hoang Phuong, 1997). Our lithostratigraphic data recorded in the borehole logs
117 shows that the Pleistocene layers have a low thickness on the left bank, while they are relatively
118 thick on the right bank (Cong-Thi et al., 2021b). Sediments derived from marine-alluvial sources
119 (Hoang Phuong, 1997; Cong-Thi et al., 2021a) are composed of clean sand, clay, clayey sand,
120 clayey sand containing grits, gravels, and small rocky fragments derived from pre-host rocks.
121 Well-rounded quartz dominates while feldspar and other minerals (ilmenite, limonite, mica) are
122 present as minor components in the lithological units (Cong-Thi et al., 2021b).

123 The Holocene sediments were dominantly accumulated through the Flandrian
124 transgression during the Early-Middle Holocene and regression in the Middle-Late Holocene
125 (Hoang Phuong, 1997; Tran Nghi et al., 2007). The former is supported by the profile of LK07-BT
126 and LK13-BT (Fig. 1) with the grain size decreasing gradually from clay-bearing coarser sand
127 close to the bedrock to fine clayey sand near the surface (Cong-Thi et al., 2021b). The latter is
128 proven by grain-sized descriptions of LK01-BT, LK17-BT, and LK19-BT. The Holocene layer
129 with a thickness of 2 m to 20 m is characterized by alternating sedimentary layers of varying

130 compositions: such as sandy layers with interbedded clayey sand, and sandy clay layers,
 131 sometimes including fine-grained silt. The lithological composition including arkose and lithic-
 132 arkose sand was possibly connected to the sandy debris derived from the magmatic arcs,
 133 subduction complex, and eroded granitoid in the older tectonic setting (Dickinson, 1979; Miall,
 134 2009) and complemented by deposition formed in lagoons that were forming a group of alluvial-
 135 marine transition facies (Nguyen Van Vuong, 1991; Hoang Phuong, 1997). Moreover, the local
 136 presence of multi-colored clay lenses forming locally aquitard units and containing black humus
 137 is characteristic of this period.

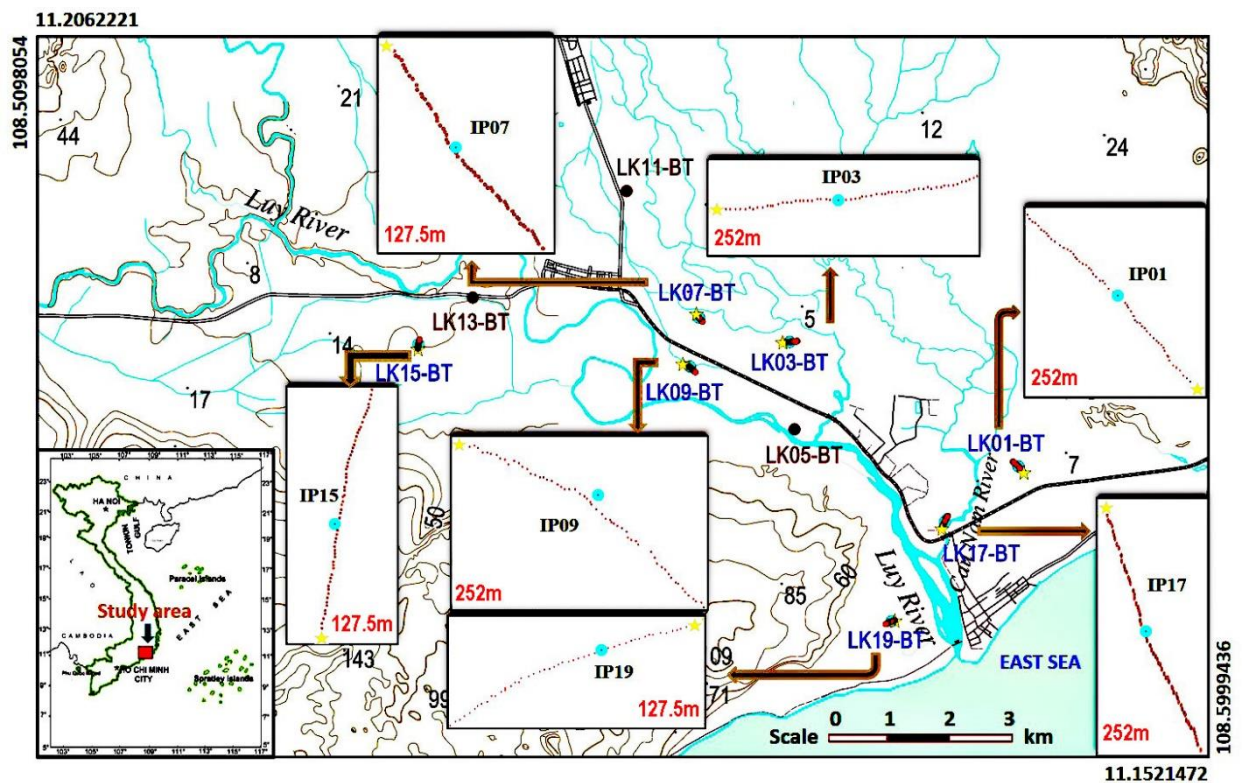


Figure 1: Location of the study site. Boreholes are indicated by brown and blue circles. Geophysical measurements coincide with the green boreholes. Yellow stars indicate the first electrode in geophysical lines whose lengths are specified in red. The analyzed unconsolidated samples were collected from these boreholes.

138 The transgressive and regressive cycles induced repeated sea-level changes combining
 139 depositional and erosional effects, and sedimentary discontinuity, resulting in lowstand,
 140 transgressive, and highstand systems tracts (LST, TST, HST respectively) (Tran Nghi et al., 2007).

141 Obviously, the sea-level changes played a vital role in the variation of the sedimentary
142 compositions and the presence of seawater in aquifers. Recent hydrogeological investigations
143 revealed that the aquifer system is experiencing a long-term freshening trend, likely since the last
144 water highstand, but is locally affected by salinization resulting from anthropic activities (Dieu et
145 al., 2022). Paleo-seawater has been entrapped in the clay-rich sediments, the heterogeneous nature
146 of sediments therefore plays a major role in the distribution of salinity in the study area (Dieu et
147 al., 2022).

148 **3. Methodology**

149 **3.1. Laboratory measurement**

150 *3.1.1. SIP measurement configuration*

151 To scrutinize the petrophysical relationships of the porous sediments, the complex
152 electrical conductivity of each various grain-sized category is first investigated at the laboratory
153 scale through SIP measurements. We rely on the SIP system proposed by Zimmermann et al.
154 (2008) using the four-point measurement method represented by two electrodes for current
155 injection and two other electrodes for potential differences (Appendix A). A polyvinyl chloride
156 sample holder 32 cm long with a 3 cm inner diameter was employed. The potential (brass)
157 electrodes were spaced 12.5 cm from the current electrodes, 7 cm apart (twice the inner diameter
158 of the sample holder), and retracted from the sample to reduce polarization effects and phase errors
159 to the resolution limit of the system (< 0.1 mrad below 1 kHz, (Zimmermann et al., 2008; Revil
160 and Skold, 2011)). Current electrodes were inserted across the whole section perpendicular to the
161 main axis of the sample holder. In order to further reduce phase inaccuracy, we verified that the
162 contact impedance was smaller than the sample impedance (Zimmermann et al., 2008).

163 Two separate procedures are used for the clay-free and clay-bearing samples. Clean sand
164 with natural moisture was compacted into the sample holder to obtain a homogenous density. The
165 filled sample column was fully saturated under five different electrolytes (NaCl solution) of

166 respective conductivity 2.59 mS.m⁻¹, 25.2 mS.m⁻¹, 392 mS.m⁻¹, 1793 mS.m⁻¹, and 5560 mS.m⁻¹
167 corresponding to deionized, fresh, slightly brackish, brackish, and saline water respectively. The
168 three first solutions correspond to low and moderate salinity conditions while the two remaining
169 values represent higher saline conditions. To avoid the effect of the accumulative salts stemming
170 from the earlier saturation, the measurements were performed from the lowest to the highest
171 salinity. Water was injected into the sample until the electrical conductivity of the output water
172 was stable and in equilibrium with that of the input. For clay-bearing mixtures having clay content
173 from 15% to 35%, water injection within the column was impossible because of the low
174 permeability of the sample. Therefore, we saturated the sample with the respective solutions before
175 inserting them into the sample column.

176 In addition, the recorded electrical conductivity values were also corrected for temperature
177 (Hayasi et al., 2004; Hermans et al., 2014; Hermans et al., 2015) to 20°C, considering a 2%
178 increase of electrical conductivity per degree Celsius.

$$\sigma_{20^{\circ}\text{C}} = \frac{\sigma_{rec}}{1+0.02(t_{rec}-20)} \quad (1)$$

179 where σ_{rec} (in S.m⁻¹) is the electrical conductivity recorded in saturated conditions of the
180 temperature t_{rec} (°C) and $\sigma_{20^{\circ}\text{C}}$ (in S.m⁻¹) is the corrected electrical conductivity at 20°C.

181 The complex conductivity and phase shift are investigated at the voltage of 5 V and the
182 frequency in an interval range from 1 Hz to 45000 Hz. However, during processing, we prioritize
183 the low-frequency range under 1000 Hz, particularly at 1 Hz due to their stability and sensitivity
184 to salinity. For all salinities, three replicates were investigated. We also measured both reciprocal
185 and normal measurements to estimate the error. The reciprocal measurements were performed
186 prior to normal measurements. A reciprocal measurement is a procedure where current and
187 potential electrodes are switched. The voltage difference applied during the reciprocal
188 measurement was of lower intensity to stay close enough to the current-free electrode impedance.
189 It was usually ± 0.1 V instead of ± 5 V (Huisman et al., 2016).

190 An essential point in the evaluation of the complex electrical conductivity is the assessment
 191 of the geometrical factor of the sample holder (Revil et al., 2017). To translate a measured complex
 192 impedance to a complex electrical conductivity, this factor depends on the position of electrodes
 193 which affects the current distribution between the current electrodes and the geometry of the
 194 sample holder. We determined the geometric factor by filling the column with the saline solutions
 195 of known conductivity only (no solid matrix) and measuring the impedance with the mentioned-
 196 above SIP configuration. The geometrical factor of our sample holder is 0.01357 m.

197 3.1.2. Sample preparation

198 Particle size distribution analysis (PSD) (Wentworth, 1922) using both wet and dry standard
 199 sieving techniques as stipulated in the American Society for Testing and Materials (ASTM D422-
 200 63) was first applied to sort unconsolidated sediments. Fifty-five disturbed samples collected from
 201 ten drilled boreholes coinciding with the geophysical measurements (Fig. 1) were classified into
 202 four groups: three clay-free categories composed of clean sand (fine-, medium-, and coarse-
 203 grained sand) and a clay-bearing mixture category. In addition, the finer suspended particles of the
 204 2 μm fraction were also analyzed through X-ray diffraction. It revealed the mineralogical content
 205 of the clay fraction mainly containing an aggregate of kaolinite, illite, chlorite, and a smaller
 206 quantity of goethite (Table 1).

207 Table 1: Summary of the results of X-ray diffractograms

Order. No	Sample. No	Mass (gram)	Components and content (%)						
			<i>Illite</i>	<i>Kaolinite</i>	<i>Chlorite</i>	<i>Quartz</i>	<i>Potassium Feldspar</i>	<i>Goethite</i>	<i>Others</i>
1.	LK07-BT (0-13m)	58.31	18-20	7-9	1-3	51-53	9-11	4-6	-
2.	LK07-BT (13-15m)	58.46	15-17	12-14	3-5	48-50	8-10	3-5	Amphibole, Lepidolite, Calcite

208 3.1.3. Complex conductivity (σ)

209 Complex conductivity (σ) can be expressed as :

$$\sigma(\omega) = \sigma'(\omega) + i\sigma''(\omega) = |\sigma|e^{i\varphi} \quad (2)$$

1
2
3
4
5 210 with $|\sigma| = \sqrt{\sigma'^2 + \sigma''^2}$ the amplitude, $\varphi = \text{atan} \frac{\sigma''}{\sigma'}$ the phase shift, σ' the real or in-phase
6
7
8 211 component related to the ohmic conduction properties and σ'' the imaginary or out-of-phase
9
10 212 component linked with the capacitive and inductive properties. For small phase shifts as the ones
11
12 213 observed for consolidated and porous sediments (<100 mrad), phase shifts can be estimated as the
13
14
15 214 ratios:

$$\varphi_r(\omega) \approx \left(\frac{\sigma''(\omega)}{\sigma'(\omega)} \right) \quad (3)$$

16
17
18
19
20
21
22 215 where ρ is the resistivity, the reciprocal of conductivity σ . This approximation equation is fairly
23
24 216 valid for metal-free soils and rocks (Heenan et al., 2013). For this reason, it is valid for the
25
26
27 217 unconsolidated sediments in the Luy River catchment which contains clay-bearing mixtures and
28
29 218 will be influenced by electrically charged grain surfaces (Kemna, 2000; Schön, 2011; Saneiyani et
30
31
32 219 al., 2018).

33
34
35 220 At low frequencies comparable to field surveys of time-domain IP (<10 Hz), we may
36
37 221 neglect the effect of the complex permittivity ε^* so that the effective in-phase conductivity and the
38
39
40 222 effective quadrature conductivity corresponds to σ' and σ'' (Kremer et al., 2016). For higher
41
42 223 frequencies, the displacement current has to be taken into account through the dielectric
43
44
45 224 permittivity.

46
47 225 When electronic semi-conduction or metallic conduction can be neglected, i.e. in the
48
49
50 226 absence of metal-bearing grains, the conductivity may be described in terms of the electrolyte
51
52 227 conduction, which may be regarded as affecting only the real part of conductivity in parallel with
53
54
55 228 interfacial conduction, which affect both the real and the imaginary parts of conductivity (Kemna,
56
57 229 2000).

$$\sigma = \sigma_{el} + \sigma_{int} = \sigma_{el} + \sigma_s \quad (4)$$

58
59
60
61
62
63
64
65

230 Archie's law can be used to empirically quantify the electrolytic conduction σ_{el} (Archie,
 1 231 1942; Schön, 2011), which for a saturated medium is given by:

$$\sigma_{el} = \frac{\sigma_f}{F} = \frac{\Phi^m}{a} \sigma_f \quad (5)$$

8 232 The formation factor ($F = \frac{a}{\Phi^m}$) is also inversely proportional to pore textural properties,
 9
 10
 11 233 namely the cementation exponent (m) and porosity (ϕ) (Schön, 2011), while a is an empirical
 12
 13 234 factor that should be equal to one.

16 235 The complex interfacial conductivity can be expressed for a saturated medium as (Börner
 17
 18
 19 236 et al., 1996):

$$\sigma_{int} = \frac{h(\sigma_f) S_{por}}{F} (1 + il) \quad (6)$$

26 237 where $h(\sigma_f)$ is a nonlinearly real function of salinity, S_{por} refers to the specific surface
 27
 28 238 area related to pore volume, and F presents the formation factor. The $l = Im(\sigma_{int}) / Re(\sigma_{int})$
 29
 30
 31 239 accounts for the actual separation of σ_{int} into real and imaginary parts and generally varies from
 32
 33 240 0.01 to 0.15 (Börner et al., 1996). Since the electrolytic conductivity is a real quantity, the
 34
 35
 36 241 interfacial properties can be accessed through the imaginary part of σ'' which depends on $Im(\sigma_{int})$
 37
 38 242 whereas the real part of σ' relates to both the electrolytic and interfacial conduction.

41 243 As the pore fluid conductivity (σ_f) decreases and tends towards zero, the real part of σ' may
 42
 43
 44 244 allow to access the real part of the interfacial conductivity or surface conductivity (σ_s).

47 245 *3.1.3. Correlation between time-domain chargeability and complex electrical quantities*

50 246 It is standard to fit a Cole-Cole model to relate the induced polarization effects in the time
 51
 52 247 domain with the observations in the frequency domain (Everett, 1997). Indeed, the Cole-Cole
 53
 54
 55 248 model is an accepted complex conductivity/resistivity model expressed by the normalized
 56
 57 249 chargeability (M_n), the frequency dependence (f or ω), and the time constant (τ) (Kemna, 2000)
 58
 59 250 as follows:

$$\sigma_c = \sigma_\infty - \frac{M_n}{1 + (i\omega\tau_0)^c} \quad (7)$$

$$M_n = \sigma_\infty - \sigma_0 \geq 0$$

where M_n defines the normalized chargeability, c refers to the frequency exponent ($0 \leq c \leq 1$), τ_0 represents the relaxation time (or time constant) in seconds and σ_0 and σ_∞ define the electrical conductivity at low frequency and high frequency, respectively. In addition, M_n is a function of the conductivity (σ'') in the imaginary part.

Following the methodology of Revil (2017), the normalized chargeability is correlated with the quadrature conductivity measured at (or close to) the relaxation peak.

$$\sigma'' = -\frac{1}{2} \frac{M_n \cos[\frac{\pi}{2}(1-c)]}{\cosh[c \ln(\omega\tau_0)] + \sin[\frac{\pi}{2}(1-c)]} \quad (8)$$

At the critical frequency $\omega = 1/\tau_0$, $0 \leq c \leq 1$ and with c fixed to 0.5 for uniform ranges of grain-sized particles and smaller for broad sizes, σ'' is intimately related to M_n by:

$$\sigma'' = -\frac{1}{2} \frac{M_n \cos[\frac{\pi}{2}(1-c)]}{\cosh[c \ln(\omega\tau_0)] + \sin[\frac{\pi}{2}(1-c)]} \quad (9)$$

$$\sigma'' = -\frac{1}{2} \frac{\cos[\frac{\pi}{2}(1-c)]}{\sin[\frac{\pi}{2}(1-c)]} M_n \quad (10)$$

$$\sigma'' = -\frac{1}{2} \left(\frac{\sqrt{2}}{1+\sqrt{2}} \right) M_n \approx -\frac{1}{5} M_n \quad (11)$$

M_n is considered to be approximately 5 times σ'' (Revil et al., 2015). In other words, M_n is not only quantified by the intensity of surface polarization but also is proportional to σ'' . For non-metallic media, σ'' is closely associated with surface chemistry and lithology (Slater and Lesmes, 2002).

3.2. Field measurement

ERT and TDIP imaging were performed on 7 profiles collected in both upstream and downstream parts along the Luy River. All mid-points of profiles coincide with the boreholes where the samples for laboratory analysis were collected (Fig. 1).

With the goal of validating the petrophysical relationship accounting for clay and obtaining a good signal-to-noise ratio, the ABEM Terrameter LS1 equipment using dipole-dipole configuration including 64 electrodes was used in each profile with 2.5 m and 4 m separation between electrodes depending on the depth of the drilled boreholes. The minimum and maximum currents were 10 mA and 500 mA respectively. The acquisition delay time was set up at 0.8 seconds and the acquisition time to 1.2 seconds resulting in a total injection of 2 seconds. The TDIP signal was recorded using 20 time windows using increasing time intervals for a total recording time of 4.0 seconds. To reduce the contact resistance and maintain a reliable signal-to-noise ratio throughout the investigation sequences, saltwater was poured at the locations of the electrodes buried under dry sand conditions. The acquisition protocol was sorted to avoid the electrode polarization effect (Dahlin et al., 2002).

Prior to inversion, the negative resistance values and chargeability exceeding 1000 MV/V, that are considered physically impossible (Loke, 2011) were removed, and noisy decay curves were removed manually (Evrard et al., 2018). Relying on the methodology proposed by Slater et al. (2000), data quality was also assessed for 6 profiles based on reciprocal measurements. A threshold of 1% was selected to filter the data sets for all profiles, except for the reciprocal error in profile LK19-BT, for which 5% was selected. The dataset is inverted in RES2DINV (Loke and Baker, 1996). The L1-norm was used for both the model constraint to promote sharper resistivity contrasts (Cong-Thi et al., 2021a) and the data constraint to limit the impact of possibly remaining outliers.

289 Electromagnetic induction (EM39, Geonics©) was used to collect vertically detailed logs
1 290 of the electrical conductivity in 9 drilled boreholes equipped with non-conductive PVC casing
2
3 291 (Vandenbohede et al., 2008). The probe operates at a frequency of 39.2 kHz with a coil spacing of
4
5
6 292 0.5 m (Mc Neill, 1990).
7

8
9 293 Before each logging, the calibration procedures were applied to verify that the probe was
10
11 294 solely measuring zero conductivity. Data were collected in the vertical direction using a distance
12
13
14 295 interval of 0.2 m. The collected data were validated in both up and down directions. The inner
15
16 296 diameter of the boreholes is 60 mm so that the influence of the borehole fluid and casing should
17
18
19 297 be minimized, as the sensitivity of the probe is maximum at a radial distance of 30 cm from the
20
21 298 probe center (McNeil et al., 1990).
22
23

24 299 **4. Results**

27 300 **4.1. Laboratory results**

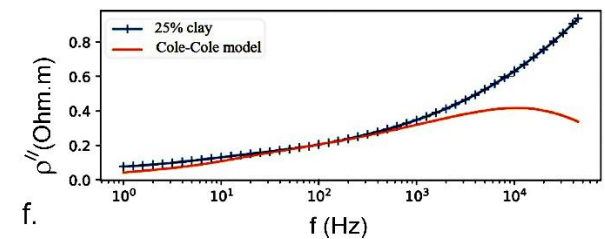
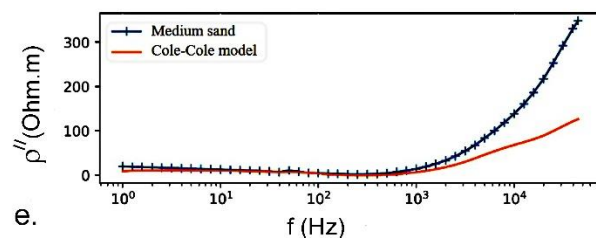
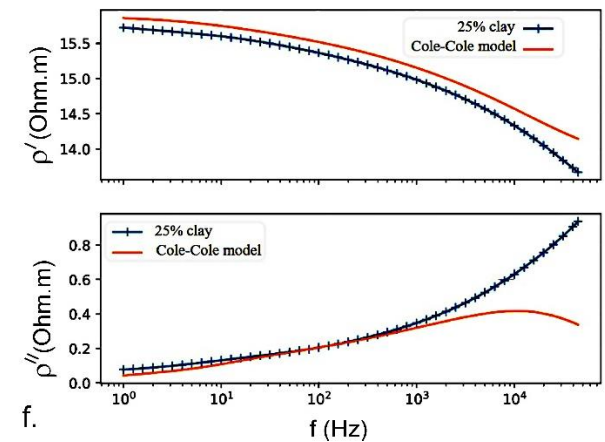
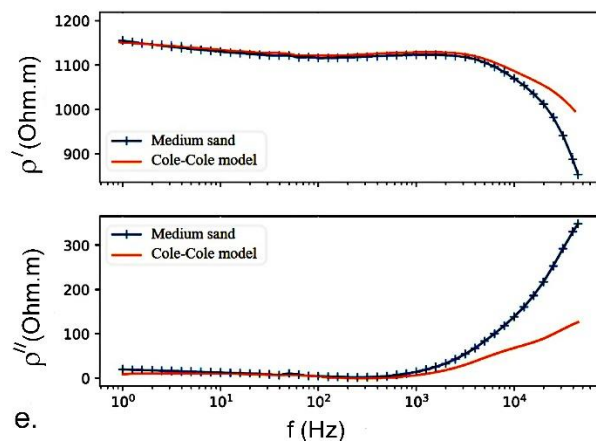
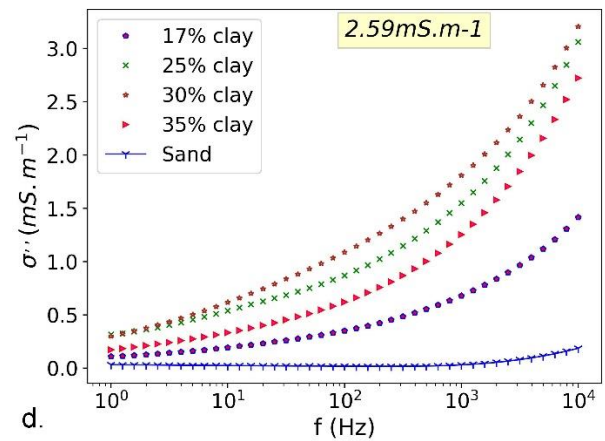
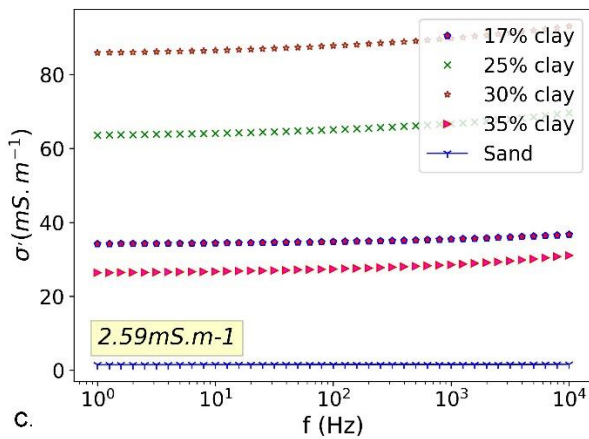
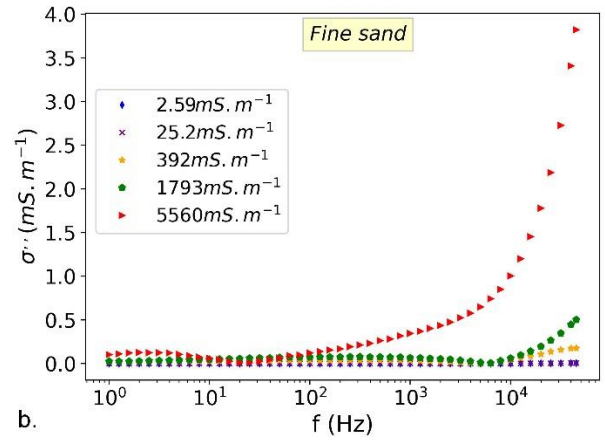
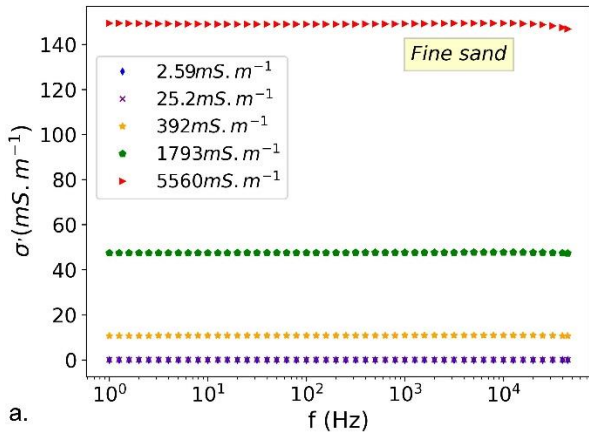
30 301 *4.1.1. SIP*

33 302 Figures 2a and b show a significant influence of the NaCl concentration on the spectra of
34
35
36 303 both real (σ') and imaginary (σ'') conductivity. Besides, the dependence of the out-of-phase
37
38 304 component is simultaneously observed at a higher frequency of 1000 Hz (Fig. 2b). As expected,
39
40
41 305 higher saline concentration corresponds to higher magnitudes of complex conductivity (Fig. 2a),
42
43 306 whereas the opposite trend is observed for the phase (Appendix B). In addition, no peak is observed
44
45
46 307 in the complex conductivity spectra. This might be explained by the non-uniform grain size of the
47
48 308 sandy materials. Figure 2c and d illustrate the influence of the presence of clay minerals, increasing
49
50
51 309 both the real and imaginary conductivity components, particularly for low salinity. This increase
52
53 310 is dependent on the clay content of the samples.

54
55
56 311 The sample containing 35% has a lower conductivity than expected, this could be caused
57
58 312 by an increase in the cementation exponent. Natural clay in sediments can play a considerable role
59
60
61 313 as cement in the pore space of sandy sediments, resulting in reducing the porosity and pore-

62
63
64
65

314 connectivity, particularly surface ionic mobility. Furthermore, the surface conductivity caused by
 1 315 charged ion mobility in the EDL dominates the complex conductivity. This phenomenon also
 2
 3 316 affects the quadrature conductivity component. In other words, the mixture containing a large
 4
 5 317 proportion of clay minerals seems to be more compacted, reducing the cation exchange capacity
 6
 7
 8 318 (CEC) of clay. This effect might have been induced by the sample preparation.



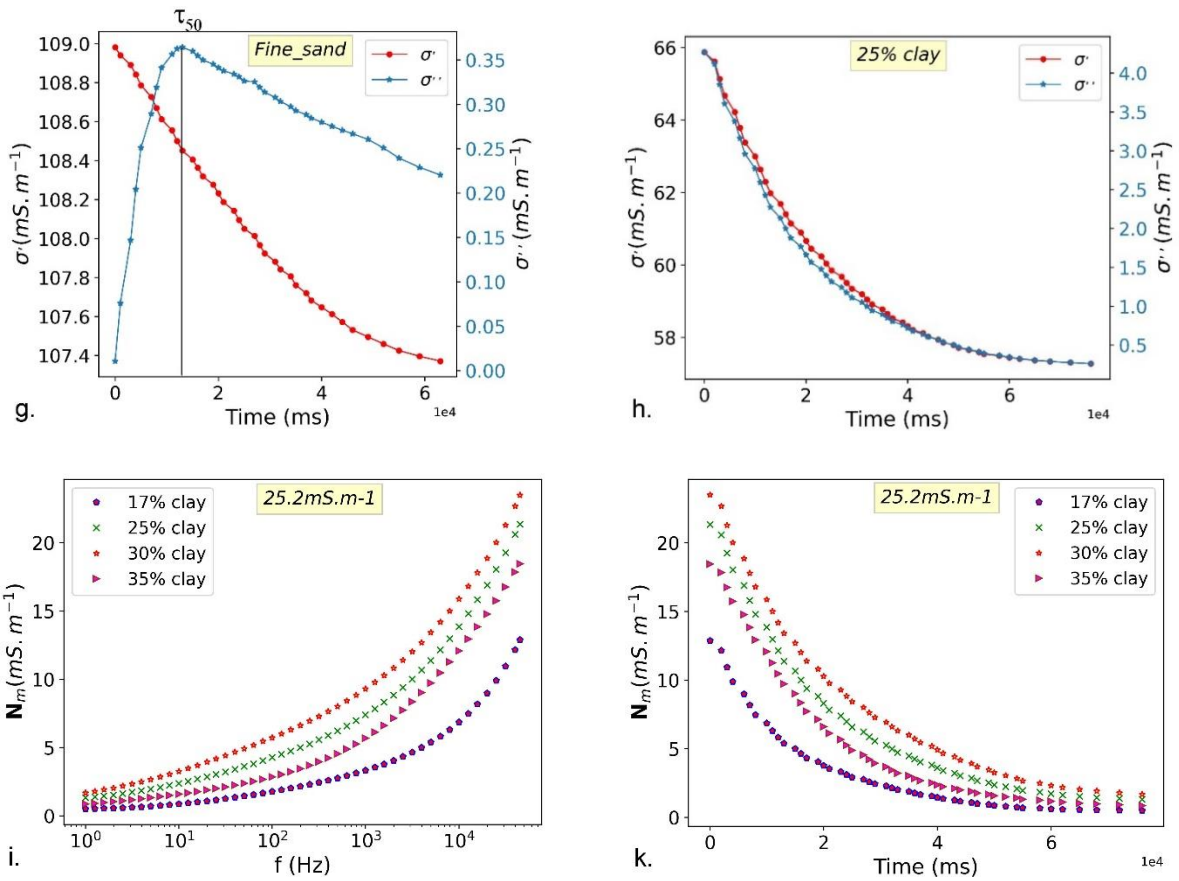


Figure 2. a. The in-phase (σ') and b. out-of-phase (σ'') conductivity components of the representative clean sand category for different salinities. Effects of clay content with respect to the surface conductivity at the lowest salinity, corresponding to deionized water on the amplitude of the in-phase (c) and out-of-phase components (d). Fitting with the Cole-Cole model for fine sand (e) for 25% clay-bearing sand (f). The peak of the synthetic SIP data in terms of real and quadrature conductivity, for fine sand (g) and clay-bearing sand (h). Normalized chargeability against frequency (i) and time (k).

319 The Cole-Cole model approach was used to fit the measured SIP curves of all clay-free
 320 and clay-bearing categories using PyGIMLI. Figures 2e and 2f show the IP spectra of the
 321 representative samples for fine sand and clayey sand (25% clay), with the c exponent equal to 0.5.
 322 The decomposition fits the curve of fine sand more accurately than that of the clay-bearing sample.
 323 For the imaginary component, except for the well-fitted spectra of the quadrature component under
 324 1000 Hz, a partition of the spectra is not well-fitted by the Cole-Cole model at frequencies above
 325 1000 Hz. The reason could be the potential effect of the roughness of the grains in polarization
 326 conditions of the grain-pore water interface and the dielectric effect (Leroy et al., 2008; Revil,
 327 2014).

328 Figure 2g and 2h illustrate the two-phase component spectra of real and quadrature
1 329 conductivity on time scales. A peak is observed in the spectrum of the fine sand sample in a time
2
3 330 interval of 1-2 ms, which is the relaxation time τ_{50} at which 50 percent of the total chargeability is
4
5 331 reached (Weigand and Kemna, 2016). Inversely, no clear dominant relaxation time is observed for
6
7
8 332 the broad grain-sized clay-bearing sample. As mentioned earlier, this might be associated with the
9
10
11 333 surface roughness effects and the superposition of particles, widening the relaxation time (Sara
12
13 334 Johansson, 2020).

16 335 The normalized chargeability is also plotted against frequency and time as cumulative
17
18 336 curves (Eq. 11, Fig. 2i and k). The normalized chargeability varies proportionally with the
19
20
21 337 increased clay content. For the low-frequency range around 1 Hz, a threshold value for the
22
23 338 normalized chargeability around $1.5 \text{ mS}\cdot\text{m}^{-1}$ can be used to validate the presence of clay.

26 339 *4.1.2. Petrophysical relationship*

29 340 To estimate the relation between the real conductivity, the pore fluid conductivity and the
30
31
32 341 interfacial conductivity, we rely on equations 4 and 5. Figure 3a shows two different trends for
33
34 342 clay-bearing and clay-free samples. For the clean sand category, a visibly straight line shows the
35
36
37 343 nearly linear dependence of the in-phase conductivity on the pore water conductivity. Inversely, a
38
39 344 non-linear relationship is clearly observed in the clay-bearing mixtures, particularly for low
40
41
42 345 salinities. In this condition, the real bulk conductivity is not only dependent on the pore fluid
43
44 346 conductivity but also influenced by surface conductivity, which even dominates due to mobile ions
45
46
47 347 in the EDL. The general tendency of the relationship observed is a linear portion at high salinity
48
49 348 with a non-linear transition at lower salinities. Particularly, the curve approximately approaches a
50
51 349 constant, which represents the surface conductivity at low salinity.

54 350 The increased clay content in the range 17%-30% yields a growing influence of the surface
55
56
57 351 conductive values on the amplitude of the intercept as observed in Fig. 3b. The sample with 35%
58
59 352 clay does not follow this trend as explained above.

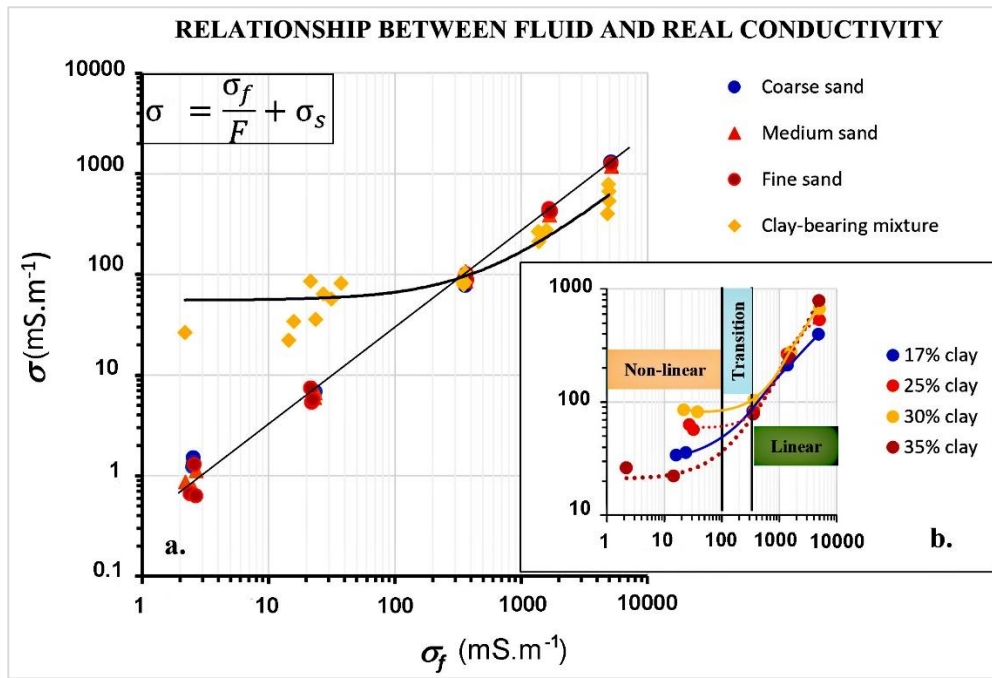


Figure 3. Log-log plot of the pore fluid conductivity versus the real conductivity. (a). A straight line represents the clean sand category (including coarse-, medium- and fine particles) and a curve refers to the clay-bearing mixture. (b). the generally detailed trends between σ and σ_f of four clay-bearing samples indicate linear relationships at higher salinity and non-linear relationships at lower salinity.

The formation factor F is the reciprocal of the slope in the linear portion, and the surface conductivity σ_s is the intercept part. (Table 2). The surface conductivity of clay-bearing sand is up to 40 times larger than that of clay-free sediments.

Table 2. Formation factor and surface conductivity of four sedimentary groups in the Luy River

Category		F	σ_s (mS.m ⁻¹)
Clay-free sediments	Coarse sand	4	2
	Medium sand	4.4	6
	Fine sand	4.1	5
Clay-bearing sediments	17% clay	13.4	55
	25% clay	10.3	71
	30% clay	8.3	76
	35% clay	6.4	21

	Mean	8.9	55
--	------	-----	----

Based on the petrophysical relationship, it is possible to define resistivity threshold values corresponding to freshwater and saline water transitions (based on 1000 and 3000 mg/L TDS limits, Cong-Thi et al., 2021a) for the four porous sediment groups calculated using equations 4 and 5 and the fitted parameters. Water electrical conductivity is converted into TDS values using a linear relationship (Keller et al., 1966; Cong-Thi et al., 2021a). Due to the uncertainty in the formation factor resulting from the different samples, we use conservative rounded threshold values (Table 3). For the sand categories, resistivity under 9 Ohm.m corresponds to saline conditions (> 3000 mg/L), and resistivity above 25 Ohm.m indicates freshwater (< 1000 mg/L). The intermediate interval corresponds to brackish water. Analogously, the threshold values for the clay-bearing mixture are 9 Ohm.m and 14 Ohm.m for saline and freshwater conditions respectively. Remarkably, these values are in agreement with the estimation of Cong-Thi et al., (2021a) made in the absence of co-located data.

Table 3. Resistive threshold values for the Luy River sediments in different salinity conditions

Category	Resistivity threshold (Ohm.m)	Condition
Clay-free sediments	>25	Fresh
	9-25	Brackish
	<9	Saline
Clay-bearing sediments	>14	Fresh
	9-14	Brackish
	<9	Saline

4.2. Field results

4.2.1. Resistivity and TDIP

372 Assuming that laboratory samples are representative for field conditions, the threshold
1 373 values computed at the laboratory scale can be used for the field scale interpretation, and combined
2
3 374 with borehole logs to characterize the complex distribution of heterogeneous sediment sequences.
4
5
6 375 An example is given in Fig. 4 and 5 for two selected profiles (IP07 and IP03). Near the surface,
7
8 376 since unsaturated and freshwater conditions dominate, the observed resistivity varies laterally from
9
10
11 377 5 Ohm.m to 45 Ohm.m in both profiles, indicating clay-dominated lithology as confirmed by the
12
13 378 respective lithologs (LK07-BT and LK03-BT). Deeper, in IP07 lower resistivity values varying
14
15 379 from 1.5 Ohm.m to 3 Ohm.m are visible at depths from 5 m to 14 m. The lithology is relatively
16
17
18 380 homogeneous, corresponding to sandy clay under saline conditions. In IP03, a decrease of
19
20 381 resistivity values at depths between 3 m and 15 m from 16 Ohm.m to 4 Ohm.m from the right part
21
22
23 382 to the left part of the figure seems inversely proportional to the higher clay content, as corroborated
24
25 383 by the higher normalized chargeability from 3 mS.m⁻¹ to approximately 4.5 mS.m⁻¹. This reveals
26
27
28 384 that surface conduction mechanisms of disseminated clay particles play a significant role in low
29
30 385 resistivity. The high values of the normalized chargeability observed at the bottom of a borehole
31
32
33 386 in IP07 might be related to the high clay content along the whole litholog although the presence of
34
35 387 artefacts of inversion is possible. The borehole might not be representative of the lithology along
36
37
38 388 the whole profile as the chargeability anomaly is centered on the location of the borehole.
39
40
41
42
43
44
45
46
47
48
49
50
51
52
53
54
55
56
57
58
59
60
61
62
63
64
65

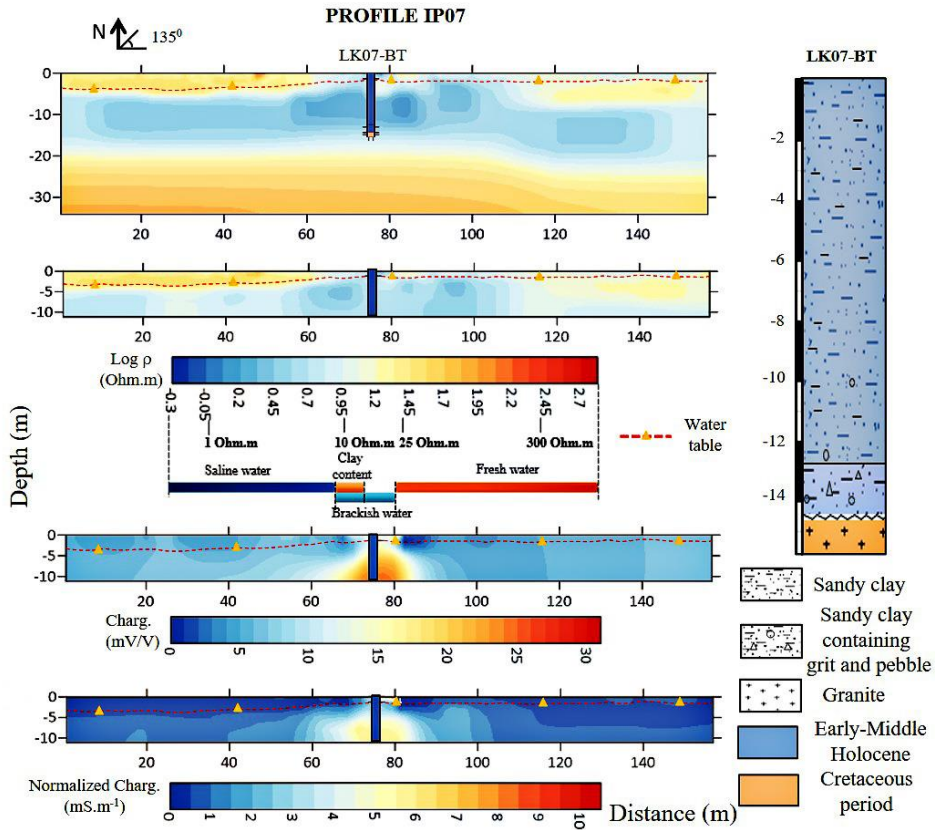


Figure 4: Inverted resistivity, chargeability and normalized chargeability of IP07 in correlation with lithostratigraphical logs in boreholes LK07-BT. Lower is the mapping of chargeability/ normalized chargeability. The broad variation of chargeability in profiles shows the more complicated distribution of clay content in the inhomogeneous context of lithology. Root-mean-squared (RMS) errors of IP07 chosen at 5 consecutive iterations are 1.28% in resistivity inversion and in chargeability map, respectively.

389 The transition between the unconsolidated sediment layers and unaltered bedrock is
 390 characterized by the rapid increase of resistivity ranging from 50 Ohm.m to 150 Ohm.m. For both
 391 profiles, the bedrock is identified as expected by an increase in resistivity. The discrepancy in the
 392 depth is likely linked to the smoothing effect of inversion (Cong-Thi et al., 2021a).

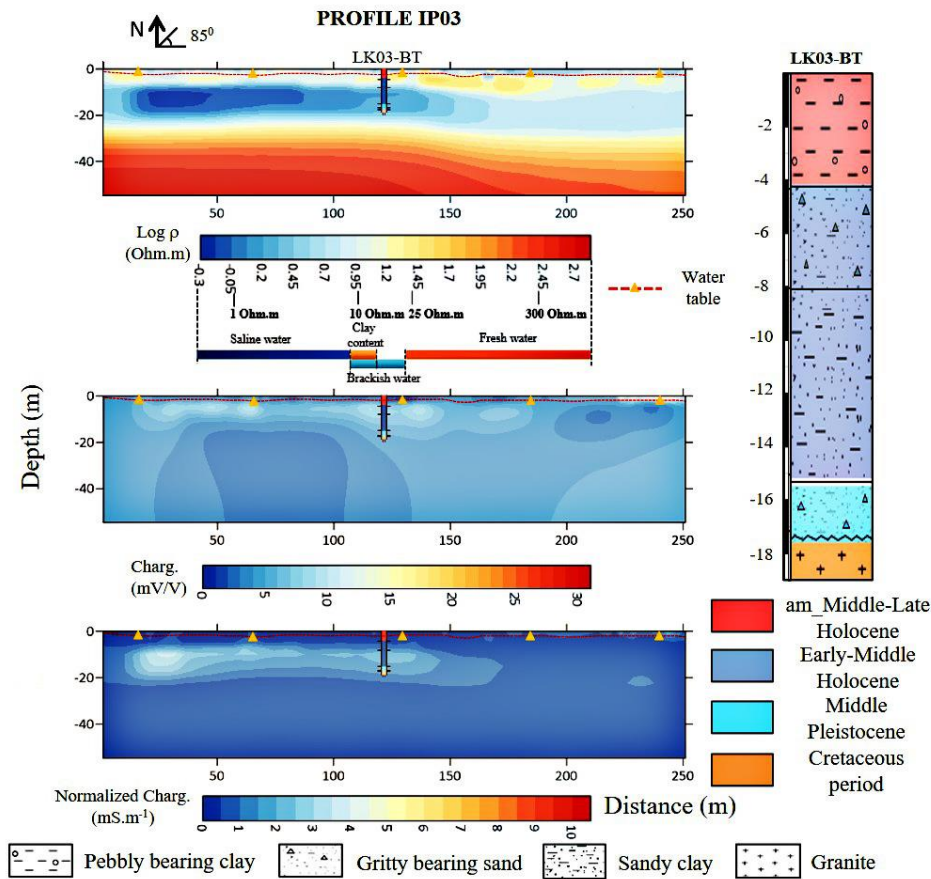


Figure 5: Similar to IP07, the inverted resistivity, chargeability and normalized chargeability of IP03 in correlation with lithostratigraphical logs in boreholes LK03-BT. Lower is the mapping of chargeability/normalized chargeability. Higher normalized chargeability indicates the presence of clay content. Root-mean-squared (RMS) errors of IP03 chosen at 5 consecutive iterations is 0.97% and 0.44% in resistivity inversion and in chargeability maps, respectively.

4.2.2. Correlation between EM39 and ERT data

To validate the variations of the resistivity in the heterogeneous sediment layers, we provide a comparison of the inverse solutions with co-located data by computing the average recorded value in EM39 logs within the corresponding ERT block depth intervals. Averaging within a block allows to partly account for the different investigated volumes (Benoit et al., 2018).

Overall, ERT can reproduce relatively well the conductivity trend measured in logs (Fig. 6 and 7). Better matching between both measuring techniques is visible at low conductivity intervals from 0 to 250 mS.m⁻¹ (Fig. 6a), corresponding to fresh-brackish water conditions of TDS under 1500 mg/L (Appendix C). Most ERT-inverted conductivity values (approximately 70%) have a

402 deviation smaller than 30 mS.m^{-1} from what is measured at a higher resolution with EM39 (Fig.
 1 403 6a). This good correspondence is for example observed in LK07-BT and the shallower location (
 2
 3 404 20 m) in LK01-BT. The ERT values correctly image the gradual increase in conductivity from 150
 4
 5 405 mS.m^{-1} in LK07-BT and 80 mS.m^{-1} in LK01-BT at the depth of 8 m to higher conductivity at larger
 6
 7 406 depths (Fig. 7a and b), corresponding with what is expected in theory for clay-dominated
 8
 9
 10
 11 407 sediments. This reveals the conductive response being governed by lithology.

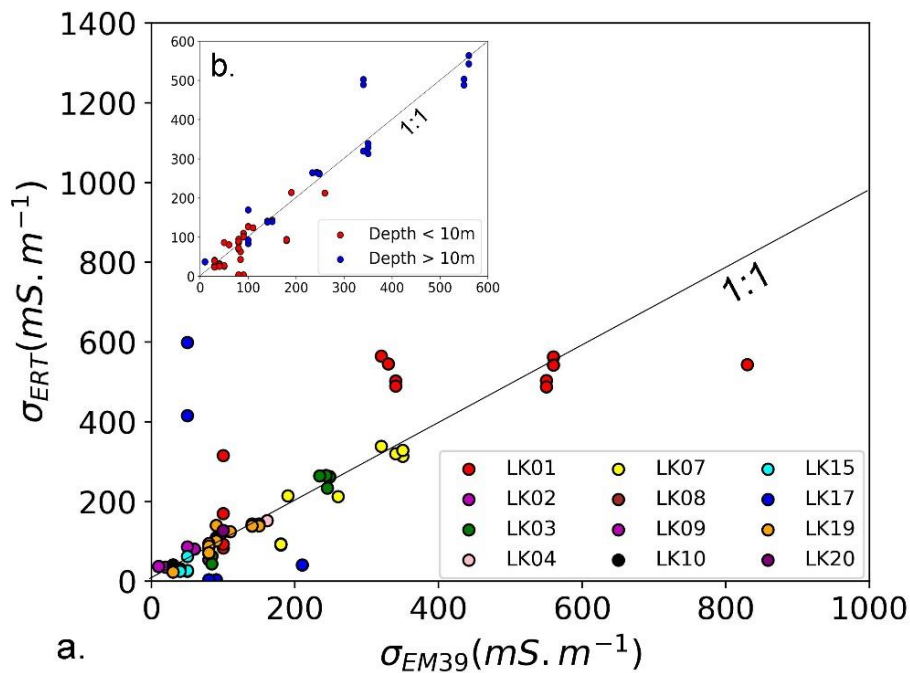


Figure 6. a. Relationship between EM39 and ERT dataset. The 1:1 line represents perfect correlation. b. Correlation between EM39 and ERT with depth. The depth division is chosen as 10m based on the averaged mid-depth point of each profile.

408 Nearly 20% of the total investigated points have a difference of $30 - 100 \text{ mS.m}^{-1}$. Such
 409 difference is for example observed between 4 m and 6 m deep in LK03-BT (Fig.7b), where a
 410 decrease in conductivity is shown from 85 mS.m^{-1} to 40 mS.m^{-1} , relatively consistent with the
 411 transition to a coarser category containing a majority of sands and a minority of clay and grit (<
 412 15%) in the lithologs. In contrast to EM39 records at this deep interval, the observed ERT values
 413 are only varying in a limited range from 45 mS.m^{-1} to 65 mS.m^{-1} . This discrepancy could be related
 414 to the limited resolution of the inversions.

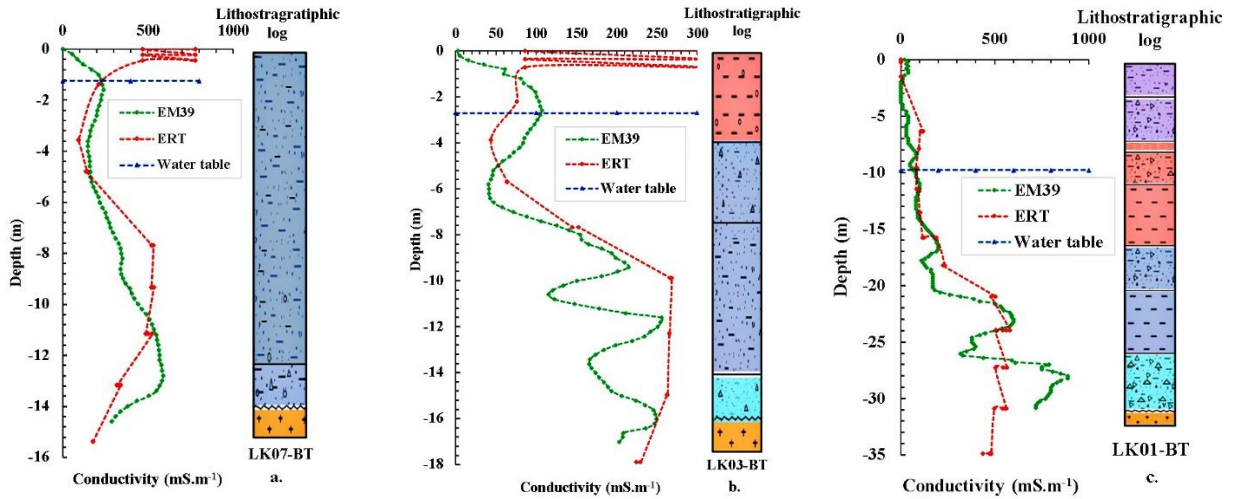


Figure 7. Conductive relationship between EM39 and ERT dataset.

415 The tendency of increase in conductivity downward to the bedrock, due to increased
 416 salinity in groundwater (Fig.7), is observed in most EM39 logs. However, this trend is not always
 417 consistent in inverted models, leading to high differences exceeding 100 mS.m^{-1} . A typical
 418 example is for the unconsolidated layers lying on granite bedrock, in LK01-BT (Fig. 7c), the
 419 increase in conductivity of EM39 reaches 900 mS.m^{-1} in the gravel layer while that of ERT is much
 420 lower (around 500 mS.m^{-1}) and varies insignificantly below the depth of 20 m. The high deviations
 421 for these data are caused by the regularization term and loss of the resolution with depth (Day-
 422 Lewis et al., 2005; Hermans and Irving, 2017), and sometimes to compensation artefacts (higher
 423 resistivity spike causing lower resistivity values below, see for example the obvious outlier in
 424 LK07-BT). These effects prevent ERT to provide an as detailed description as combined
 425 EM/lithologic logs. However, there is no clear indication that the depth can explain strongly
 426 deviating points (Fig. 6b). This implies that a diminishing depth resolution is not the only cause
 427 for deviations, but other causing factors such as the presence of inversion artefacts caused by
 428 anthropic structures at the surface, the averaging calculation methodology, and the measuring scale
 429 play a role. High deviations are also observed near the surface, at depths shallower than 1 m,
 430 conductive features in the ERT data fluctuate repeatedly from 80 mS.m^{-1} to 300 mS.m^{-1} in LK03-
 431 PT and from 450 mS.m^{-1} to 800 mS.m^{-1} in LK07-BT while EM39 in both boreholes varies slightly
 432 under 150 mS.m^{-1} . This could be related to global smoothing regularization and the above-

433 mentioned artefacts of inversion linked to anthropic structures in the vicinity of the wells (Hermans
1 434 and Irving, 2017; von Bülow et al., 2021).

2
3
4 435 Generally, the ERT and EM39 features show relatively identical trends but ERT data is
5
6 436 recorded through a larger scale and with a lowering resolution with depth, causing deviations from
7
8
9 437 EM39 data. For conductivity values under 250 mS.m^{-1} corresponding to fresher conditions, the
10
11 438 ERT inverted models reveal a more accurate quantitative estimation of the bulk electrical
12
13
14 439 conductivity. For higher conductivity values, the ERT inversion models are qualitatively correct
15
16 440 and generally sufficient to conclude the resistivity threshold for saline water.

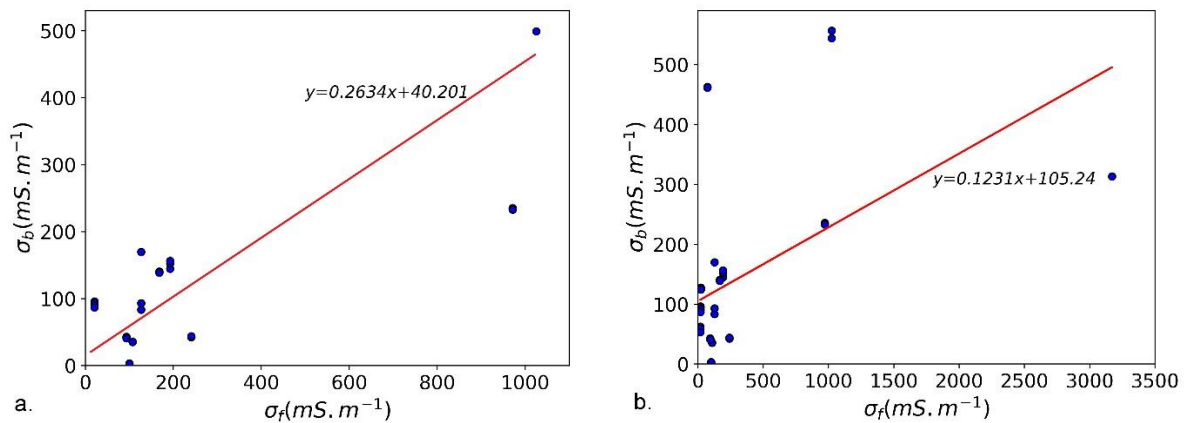
19 441 *4.2.3. Correlation between salinity and ERT data*

20
21 442 Figure 8 shows two scatterplots built from two distinct lithological categories containing
22
23
24 443 clay-free and clay-bearing layers. To avoid comparative errors in assessing the validity of the
25
26 444 petrophysical relationship obtained in the laboratory at the field scale, we extracted ERT
27
28
29 445 conductivity values in boreholes where the water conductivity was measured on groundwater
30
31 446 samples. The bulk inverted resistivity at the depth of the screen interval was averaged within a 5
32
33
34 447 m radius cylinder around the borehole location. Figure 8a represents the sandy sediment. Most
35
36 448 points have a water conductivity lower than 250 mS.m^{-1} , which makes it difficult to derive a strong
37
38
39 449 trend. Most points show a spread around the linear trend line at low conductivity values.
40
41 450 Analogously to the lab methodology, from equation 4, the formation factor and surface conduction
42
43 451 can be derived and are 3.8 and 40.201 mS.m^{-1} , respectively. The surface conductivity value is
44
45
46 452 larger than in the lab and likely accommodates the averaging nature of resistivity at this scale.

47
48 453 Figure 8b corresponds to clay-dominated samples. Here, data points are scattered over a
49
50
51 454 wide range of bulk electrical conductivity for a given water conductivity. This scattering is likely
52
53 455 an effect of the variability in the clay content of the various samples, in accordance with what was
54
55
56 456 observed for the surface conduction of laboratory samples, combined with the averaging effect of
57
58 457 ERT. Although deriving a trend is only indicative given the weak tendency, a formation factor of
59
60 458 8.1 and surface conductivity of 105.24 mS.m^{-1} are derived.

459 Remarkably, the spread in bulk conductivity observed at the low value of water
 1 460 conductivity is consistent with the expected range observed at the laboratory scale (Fig.3, Table
 2
 3 461 2), spanning almost to an order of magnitudes. Similarly, the formation factor values are acceptable
 4
 5 462 for the described lithology and in agreement with lab processing data. However, the field-scale
 6
 7
 8 463 surface conductivity is higher than the lab-scale one. This could be likely related to the
 9
 10
 11 464 heterogeneous nature of the sediment sequences in the study area (Fig. 4, 5 and 7). Indeed, the
 12
 13 465 broad grain-sized variation, fraction and dispersion of clay are responsible for deviations from the
 14
 15
 16 466 lab petrophysical relationship.

17
 18 467 The good agreement of ERT with EM39 measurements at low salinity combined to the
 19
 20
 21 468 large spread observed in the field petrophysical relationship suggests that the clay content has an
 22
 23 469 important impact on the field resistivities. ERT results can therefore be used for saltwater
 24
 25 470 delineation (high salinity threshold), but should be thoughtfully handled to derive quantitative
 26
 27
 28 471 estimates of the salinity, especially at low salinities, where the clay content dominates the response.



46
 47 Figure 8. Plotting fluid conductivity against bulk conductivity. a. for the clay-free category. b. for the
 48 clay-bearing mixture.
 49

51 472 5. Discussions

52
 53
 54 473 Through ERT/TDIP, EM39, and SIP investigations, lithological subsurface information at
 55
 56
 57 474 various scales has allowed for the interpretation of heterogeneity between the unconsolidated
 58
 59 475 sediment layers in the Luy River coastal aquifers. At the small scale, our laboratory data shows
 60
 61
 62 476 that the chargeability characterized by quadrature conductivity is proportional to the electrical
 63
 64
 65

477 conductivity of samples and increases with the clay content, except for the maximum tested clay
1 478 content (35%), which likely results from sample preparation. This is in accordance with the
2
3 479 previous studies, which generally indicate an inverse correlation between increasing polarization
4
5
6 480 and clay content with decreasing resistivity (Vacquier et al., 1957; Marshall and Madden, 1959;
7
8 481 Ogilvy and Kuzmina, 1972; Klien and Sill, 1982). In other words, the interconnection between the
9
10
11 482 quadrature conductivity and the normalized chargeability is a linear relationship (Viezzoli and Cull
12
13 483 2005; Revil et al., 2017).

16 484 In comparison with the larger scale, the field data set shows that the increase in polarization
17
18 485 response and electrical conductivity is also related to the proportion of clay content in the
19
20
21 486 petrophysical relationship (Fig. 3). The formation factor on the field scale is relatively consistent
22
23 487 with that from the SIP investigation while the field-scale surface conductivity is higher than the
24
25
26 488 lab-scale one. The discrepancy could be related to the heterogeneous distribution of sedimentary
27
28 489 layers, the coarser-sized aquifers that are alternating with argillaceous bands/lenses, and the
29
30
31 490 existence of clay minerals dispersed within the pore space, causing the increase of surface
32
33 491 conductivity magnitude (Keller and Frischknecht, 1966). Besides, the local presence of ilmenite
34
35 492 (Cong-Thi, 2021b), a conductive mineral, could affect the apparent increase in surface
36
37
38 493 conductivity. Scale and inversion effects, leading to smoothing and averaging in the resistivity
39
40
41 494 distribution, can also explain the presence of a significant surface conductivity for sand-dominated
42
43 495 sediments. In addition, the absence of extremely saline samples at the field scale made the
44
45 496 regression relatively sensitive to a few samples. The spread at low salinities is important, indicating
46
47
48 497 the difficulty to derive field-based petrophysical relationships in highly heterogeneous coastal
49
50 498 aquifers.

53 499 In the study area, in fresher conditions related to water conductivity value under 250 mS.m⁻¹
54
55 500 ¹ (TDS < 1500 mg/L), bulk conductivity seems to be governed by lithology, and the surface
56
57
58 501 conduction mechanisms of disseminated clay particles are considered to dominate over ionic
59
60 502 conduction. EM39 and ERT data generally display similar trends. However, ERT cannot detect
61
62
63
64
65

503 thin clay sedimentary layers (less than 0.5 m in Fig.7c), sometimes revealed by EM logs, due to
1 504 the poorer vertical resolution. In this range of salinity, there is a very large spread in the field-
2
3 505 based petrophysical relationship, corresponding to the large heterogeneity observed in the well
4
5
6 506 logs, preventing ERT alone to make any quantitative interpretation because of the double effect of
7
8 507 fluid salinity and clay content. In saltier conditions generally encountered at larger depths, ERT
9
10
11 508 data still display the same trend as EM logs. However, ERT cannot systematically discriminate the
12
13 509 transition between the complex sedimentary multi-layers (Fig. 7c) due to the volume-averaging
14
15
16 510 nature of ERT and the loss of resolution with depth. Nevertheless, ERT seems to be consistent in
17
18 511 predicting the salinity threshold of 9 Ohm.m for saline water (TDS > 3000 mg/L).

21 512 In terms of chargeability, low values of normalized chargeability, varying from around 1
22
23 513 mS.m^{-1} to 1.5 mS.m^{-1} , are observed where the lithological description indicates a low clay content
24
25
26 514 (<15% clay) (Fig. 4 and 5). This is consistent with the normalized chargeability between 1 mS.m^{-1}
27
28 515 1 and 1.5 mS.m^{-1} through SIP investigation of sandy samples. A threshold value of 1.5 mS.m^{-1}
29
30
31 516 seems adequate to conclude the significant presence of clay minerals. The normalized
32
33 517 chargeability in the field and laboratory scales indicates that both investigation methods reflect
34
35
36 518 quantitatively similar results. Unfortunately, there are not enough co-located samples to derive a
37
38 519 relationship between the normalized chargeability and the clay content at the field scale. Due to
39
40
41 520 the mentioned coherence, we have therefore chosen the laboratory-recorded threshold values to
42
43 521 extrapolate for the field-investigated imaging.

46 522 The normalized chargeability compared with the detailed description of lithologic and
47
48 523 EM39 logs reveals a complex distribution of clay minerals (dominated by kaolinite and illite) in
49
50
51 524 either small discontinuous lenses, locally surrounded by low resistivity zones containing
52
53 525 brackish/saline water, or in more continuous layers 0.5m to 5.5m thick, acting as regional aquitards
54
55
56 526 (Fig. 5). Clay minerals are also commonly disseminated within the sand layers (Fig. 4, 5 and 7).
57
58 527 This is often corroborated by high normalized chargeability (from 3 mS.m^{-1} to 10 mS.m^{-1}). The
59
60
61 528 normalized chargeability can be used as a first indicator for the presence of clay, and therefore to
62
63
64
65

529 discriminate between clay and salinity in the resistivity response. The IP data quality remains a
1 530 concern, as the signal-to-noise ratio is low, especially in saline conditions. Not all field profiles
2
3 531 could be inverted for the (normalized) chargeability because of the bad data quality.
4
5

6 532 The electrical response of the bedrock is also well characterized by ERT inverted models
7
8 533 (Fig. 4 and 5), based on resistivity values increasing from about 30 to 100 Ohm.m. These values
9
10
11 534 are extremely low for what is expected to be unaltered granite (> 1000 Ohm.m) (Lowrie, 2007).
12
13 535 The main contributor to this lower signal is the presence of salty groundwater (with maximum
14
15
16 536 resistivity values of 1.03 Ohm.m) within fractures. The clay content also increases at the transition
17
18 537 between unconsolidated sediments and the lower-lying bedrock, which is composed of an upper
19
20
21 538 altered granite zone. The weathering stage of the bedrock seems to vary largely between locations
22
23 539 and is superimposed with a possible presence of saltwater in the bedrock as well. Typically, the
24
25
26 540 unaltered bedrock is identified by an increase in resistivity and low normalized chargeability, while
27
28 541 weathered bedrock is difficult to discriminate from the above-unconsolidated sediments, as it is
29
30
31 542 characterized by the normalized chargeability varying from 1.5 mS.m^{-1} to 3 mS.m^{-1} and relatively
32
33 543 low resistivity. Particularly in the complexity of predominantly saline conditions, other
34
35 544 contributors decreasing the conductivity could be overshadowed. Here saltwater is the main
36
37
38 545 contributor while clay presence is a co-contributor. The latter is proven by some strong
39
40 546 chargeability anomalies that could be related to higher clay content (Fig. 4 and 5), although the
41
42
43 547 presence of artefacts in the inversion process cannot be completely disregarded (Slater, 2000; Zarif
44
45 548 et al., 2017).
46
47

48 549 However, depending on field conditions, TDIP does not always provide good and reliable
49
50
51 550 results. Artefacts and/or data noise can locally distort inversion results. Near the surface, the
52
53 551 normalized chargeability is sometimes low, even in the presence of individual clay layers (Fig. 5).
54
55 552 This difference highlights the advantage of laboratory and logging methods which are more
56
57
58 553 sensitive to lithological variations. The threshold value for both the normalized chargeability and
59
60 554 resistivity are re-used to extract clay/clay-bearing sand layers. Thus, the information obtained
61
62
63
64
65

555 through SIP measurements provides insight into subsurface heterogeneity that may not be fully
1 556 resolved through ERT and TDIP data.
2
3

4 557 **6. Conclusions**

5
6

7 558 In this paper, we investigated the electrical response of heterogeneous clay-bearing
8
9
10 559 sediments subject to saltwater intrusions both at the laboratory and the field scale. Both laboratory
11
12 560 and field results are successfully correlated with the known lithological structure of the borehole
13
14
15 561 logs and allow a more complete interpretation of the lithostratigraphic correlation. As expected,
16
17 562 the SIP data also clarify the surface conductivity of the clay-containing aggregates. Our results
18
19
20 563 suggested that SIP is able to differentiate lithological heterogeneities within unconsolidated
21
22 564 sediments and particularly in the presence of clay minerals. Surface conductivity values and
23
24
25 565 formation factors increasing from coarser sand to clay-bearing sand are consistent with theory and
26
27 566 relatively similar to the field-interpreted results. However, field petrophysical relationships display
28
29
30 567 a large scattering around the trend, indicating that quantitative estimation is subject to large
31
32 568 uncertainty.
33

34
35 569 Trends of EM logs and ERT on the field are fairly coherent. However, the ERT data are
36
37 570 recorded over a larger scale, with a lower vertical resolution, causing some deviations compared
38
39
40 571 to EM logs. These deviations can be caused by the regularization used for inversion and the loss
41
42 572 of resolution with depth. For low conductivity values under 250 mS.m^{-1} , corresponding to fresher
43
44
45 573 conditions, the ERT model provides a more accurate quantitative estimation of the bulk electrical
46
47 574 conductivity, and can be used to derive the presence of clay. However, quantitative interpretation
48
49
50 575 remains difficult because of the combined effect of salinity and clay content. The use of normalized
51
52 576 chargeability can then help to identify the presence of clay lenses/layers. For larger conductivity
53
54
55 577 values, the ERT models is able to satisfactorily identify zones where the salinity exceeds the 3000
56
57 578 mg/L threshold, but should not be use to derive absolute value of salinity.
58

59
60 579 The petrophysical analysis of the SIP, ERT, and EM data towards lithology and
61
62 580 corresponding salinity pointed out the complexity linked to the very heterogeneous nature of the
63
64
65

581 study area. Globally, high-resolution ERT/IP inversions and EM logs could discriminate
1 582 unequivocally the heterogeneity of the clay-rich zones, even from saline zones. In the case of the
2
3 583 clay-rich zones, bulk conductivity is amplified by the presence of both clay minerals and salty
4
5 584 water, leading to the overshadowed existence of clay-bearing zones. ERT/TDIP data seems
6
7
8 585 insensitive to clay lenses/layers thinner than 0.5 m, even at shallow depths, leading to possible
9
10
11 586 misinterpretation between interbedding sand layers or saline/brackish conditions. Inversely, the
12
13 587 ERT model reveals a better representation of the electrical response of the bedrock.
14
15

16 588 **Author Contributions:** D.C.T conceptualized the survey plan, processed the ERT/ IP and SIP
17
18 589 data and applied the methodology, and was responsible for writing the paper. L.P.D contributed to
19
20
21 590 the fieldwork and data processing. D.C contributed to the methodology and SIP processing. X.D.P
22
23 591 participated in the ERT/IP processing and EM39 comparison. H.D.T was responsible for sample
24
25
26 592 preparation and do grain-sized analysis. H.H.H participated in the fieldwork and the
27
28 593 conceptualization of the survey plan. N.F. and H.T conceptualized the survey plan and the
29
30
31 594 methodology and supervised the study.
32
33

34 595 **Funding:** This research is funded by The Special Research Fund (BOF), Ghent University
35
36 596 through the Ph.D. scholarships of the first two authors.
37
38

39 597 **Acknowledgements:** We deeply thank the VIGMR staff for their support on the field and grain-
40
41
42 598 sized classification. We would like to thank staff members in the laboratory of the Urban &
43
44 599 Environmental Engineering, Liège University, who assisted us in the analysis of SIP
45
46
47 600 measurements.
48
49

50 601 **Conflicts of Interest:** The authors declare no conflict of interest.
51
52

53 602 **References**

- 54
55
56 603 1. Alabi, A.A., Ogungbe, A.S., Adebo, B., Lamina, O., 2010. Induced polarization interpretation
57
58
59 604 for subsurface characterization: A case study of obadore, lagos state. Archives Physics
60
61 605 Research 1, pp. 34–43.
62
63
64
65

- 606 2. Archie, G.E., 1942. The electrical resistivity log as an aid in determining some reservoir
1 607 characteristics. *Trans AIME* 146, pp. 54–62.
2
3
- 4 608 3. ASTM D422-63,. 2007. Standard Test Method for Particle-Size Analysis of Soils, ASTM
5
6 609 International, West Conshohocken, PA.
7
8
- 9 610 4. Attwa, M., Günther, T., Grinat, M., Binot, F., 2011. Evaluation of DC, FDEM, and IP
10
11 611 resistivity methods for imaging perched saltwater and a shallow channel within coastal tidal
12
13 612 flat sediments. *Journal of Applied Geophysics* 75, pp. 656–670.
14
15
16
- 17 613 5. Baines, D., Smith, D.G., Froese, D.G., Bauman, P., Nimeck, G., 2022. Electrical resistivity
18
19 614 ground imaging (ERGI): A new tool for mapping the lithology and geometry of channel-belts
20
21 615 and valley-fills. *Sedimentology* 49, pp. 441–449.
22
23
- 24 616 6. Benoit, S., Ghysels, G., Gommers, K., Hermans, T., Nguyen, F., Huysmans, M., 2019.
25
26 617 Characterization of spatially variable riverbed hydraulic conductivity using electrical
27
28 618 resistivity tomography and induced polarization. *Hydrogeology Journal* 1, pp. 395–407.
29
30 619 <https://doi.org/10.1007/s10040-018-1862-7>.
31
32
33
- 34 620 7. Börner, F.D., Schopper, J.R. and Weller, A., 1996. Evaluation of transport and storage
35
36 621 properties in the soil and groundwater zone from induced polarization measurements.
37
38 622 *Geophysical Prospecting* 44(4), pp. 583–601.
39
40
- 41 623 8. Cole, K. S., and R. H. Cole., 1941. Dispersion and absorption in dielectrics. I. Alternating
42
43 624 current characteristics, *The Journal of Chemical Physics* 9, pp. 341–351.
44
45
- 46 625 9. Cong-Thi, D., Dieu, L.P., Thibaut, R., Paepen, M., Huu, H.H., Nguyen, F., Hermans, T.,
47
48 626 2021a. Imaging the structure and the saltwater intrusion extent of the Luy River coastal aquifer
49
50 627 (Binh Thuan, Vietnam) using electrical resistivity tomography. *Water* 2021 13, 1743 pp.
51
52 628 <https://doi.org/10.3390/w13131743>.
53
54
55
56
- 57 629 10. Cong-Thi, D., Pham Dieu, L., Huu Hieu, H., Nguyen, F., Hermans, T., 2021b. Granulometric
58
59 630 and lithological composition of sediment in the boreholes along the Luy river in Bac Binh
60
61
62
63
64
65

- 631 discs., Binh Thuan province: results and interpretation. Report. Ghent University, Belgium.
632 Unpublished.
- 633 11. Dahlin, T., Leroux, V., & Nissen, J., 2002. Measuring techniques in induced polarisation
634 imaging. *Journal of Applied Geophysics* 50, pp. 279–298.
 - 635 12. Dahlin, T., and Leroux, V., 2012. Improvement in time-domain induced polarization data
636 quality with multi-electrode systems by separating current and potential cables. *Near Surface*
637 *Geophysics* 10, 1957 pp. <https://doi.org/10.3997/1873-0604.2012028>.
 - 638 13. Dieu, L.P., Cong-Thi, D., Segers, T., Huu, H.H., Nguyen, F., Hermans, T., 2022. Groundwater
639 Salinization and Freshening Processes in the Luy River Coastal Aquifer, Vietnam. *Water* 14
640 (15), 2358 pp.
 - 641 14. Dickinson, W.R and Suczek, C.A., 1979. Plate tectonics and sandstone compositions.
642 *American Association of Petroleum Geologist* 63, pp. 2164–2182.
 - 643 15. Dukhin S.S. and Shilov P., 1974. *Dielectric Phenomena and the Double Layer in Disperse*
644 *Systems and Polyelectrolytes*. John Wiley & Sons, Inc., New York.
 - 645 16. Evrard, M., Dumont, G., Hermans, T., Chouteau, M., Francis, O., Pirard, E., Nguyen, F., 2018.
646 *Geophysical Investigation of the Pb–Zn Deposit of Lontzen–Poppelsberg, Belgium*. *Minerals*
647 8, 233 pp. <https://doi.org/10.3390/min8060233>.
 - 648 17. Everett, M.E., 1997. Transient inductive coupling of loops over near-surface clay-bearing
649 sandstones. *Society of Exploration Geophysicists 67th Ann. Internat. Mtg.* (Dallas, TX,
650 November 2-7).
 - 651 18. Hayashi, M., 2004. Temperature-electrical conductivity relation of water for environmental
652 monitoring and geophysical data inversion. *Environment Monitoring Assessment* 96, pp. 119–
653 128.
 - 654 19. Hermans, T., Nguyen, F., Robert, T., Revil, A., 2014. Geophysical methods for monitoring
655 temperature changes in shallow low enthalpy geothermal systems. *Energies* 7, pp. 5083–5118.

- 656 20. Hermans, T., Wildemeersch, S., Jamin, P., Orban, P., Brouyère, S., Dassargues, A., Nguyen,
1 657 F., 2015. Quantitative temperature monitoring of a heat tracing experiment using cross-
2
3 658 borehole ERT. *Geothermics* 53, pp. 14–26.
4
5
6 659 21. Hoang, P., 1997. Geological and Mineral Map of Phan Thiet, scale 1:50.000. Cent. Inf. Arch.
7
8
9 660 J. Geol. C-49-37-A. Accessed on: <http://idm.gov.vn/1P1NPIT/vi-VN/Ban-Do-Dia-Chat.aspx>. (In Vietnamese). Accessed available: <http://idm.gov.vn/1P1NPIT/vi-VN/Ban-Do-Dia-Chat.aspx>. (In Vietnamese).
10
11 661
12
13 662
14
15
16 663 22. Hördt, A., et al., 2016. The dependence of induced polarization on fluid salinity and pH,
17
18
19 664 studied with an extended model of membrane polarization. *J. Applied Geophysics* 135, pp.
20
21 665 408–417. <http://dx.doi.org/10.1016/j.jappgeo.2016.02.007>.
22
23
24 666 23. Hördt, A., Bairlein, K., Bucker, M., Stebner, H., 2017. Geometrical constraints for membrane
25
26 667 polarization. *Near Surface Geophysics* 15 (6), pp. 579–592. <https://doi.org/10.3997/1873-0604.2017053>.
27
28
29 668
30
31 669 24. Huisman, J.A., Zimmermann, E., Esser, O., Haegel, F.-H., Treichel, A., Vereecken, H., 2016.
32
33
34 670 Evaluation of a novel correction procedure to remove electrode impedance effects from
35
36 671 broadband SIP measurements. *Journal of Applied Geophysics*. <http://doi.org/10.1016/j.jappgeo.2015.11.008>.
37
38
39 672
40
41 673 25. Keller, G.V., Frischknecht, F.C., 1966. *Electrical Methods in Geophysical Prospecting*;
42
43 674 Pergamon Press: Oxford, UK.
44
45
46 675 26. Kemna, A., Binley, A., Cassiani, G., Niederleithinger, E., Revil, A., Slater, L., Williams,
47
48 676 K.H., Orozco1, A.F., Haege, F.H., Hördt, A., Kruschwitz, S., Leroux, V., Titov, K., and
49
50
51 677 Zimmermann, E., 2012. An overview of the spectral induced polarization method for near-
52
53 678 surface applications. *Near Surface Geophysics* 10, pp. 453-468. <http://doi:10.3997/1873-0604.2012027>.
54
55
56 679
57
58 680 27. Kemna, A., 2000. *Tomographic Inversion of Complex Resistivity-Theory and Application*.
59
60 681 Ph.D. Thesis. Ruhr Universität, Bochum, Germany.
61
62
63
64
65

- 682 28. Klien, J. D., and Sill, W. R., 1982. Electrical properties of artificial claybearing sandstone:
1 683 Geophysics 47, pp. 1593–1605.
2
- 3 684 29. Krumbein, W.C., 1934. Size frequency distribution of sediments: Journal of Sedimentary
4
5 685 Petrology 4,pp. 65-77.
6
7
- 8 686 30. Krumbein, W. C., and Sloss, L. L., 1963. Stratigraphy and sedimentation: 2nd ed., W. H.
9
10 687 Freeman, San Francisco, 660 pp.
11
- 12
- 13 688 31. Leroy, P., Revil, A., Kemna, A., Cosenza, P., Ghorbani, A., 2008. Complex conductivity of
14
15 689 water-saturated packs of glass beads. Journal of Colloid Interface Science 321 (1), pp. 103–
16
17 117. <https://doi.org/10.1016/j.jcis.2007.12.031>.
18 690
19
- 20 691 32. Lesmes, D.P. and Morgan F.D., 2001. Dielectric spectroscopy of sedimentary rocks. Journal
21
22 692 of Geophysical Research 106, pp. 13329–13346.
23
24
- 25 693 33. de Lima O.A.L. and Sharma M.M., 1992. A generalized Maxwell-Wagner theory for
26
27 694 membrane polarization in shaly sands. Geophysics 57(3), pp. 431–440.
28
29
- 30 695 34. L. Insigne, M.S., and Kim, G.S., 2010. Saltwater Intrusion Modeling in the Aquifer Bounded
31
32 696 by Manila Bay and Parañaque River, Philippines. Environmental Engineering Research 15
33
34 (2), pp. 117-121. <http://doi.10.4491/eer.2010.15.2.117>. pISSN 1225-1025 eISSN 2005-968X.
35 697
36
- 37 698 35. Loke, M.H., 2011. Tutorial: 2-D and 3-D Electrical Imaging Surveys.
38
39
- 40 699 36. Loke, M. H., Barker, R. D., 1996. Rapid least squares inversion of apparent resistivity
41
42 700 pseudosections by a quasi-Newton method. Geophysical Prospecting 44, pp. 131-152.
43
44
- 45 701 37. Lowrie, W., 2007. Fundamentals of Geophysics, second edition. Assessed available:
46
47 702 <http://ebooks.cambridge.org/ebook.jsf?bid=CBO9780511807107>.
48
- 49 703 38. Martínez, J., Benavente, J., García-Aróstegui, J.L., Hidalgo, M.C., Rey, J., 2009. Contribution
50
51 704 of electrical resistivity tomography to the study of detrital aquifers affected by seawater
52
53 705 intrusion–extrusion effects: The river Vélez Delta (Vélez-Málaga, Southern Spain).
54
55 Engineering Geology 108, pp. 161–168.
56
57 706
58
- 59 707 39. Marshall, D. J., and Madden, T. R., 1959. Induced polarization, a study of its causes:
60
61 708 Geophysics 24, pp. 790–816.
62
63
64
65

- 709 40. Magnusson, M., Fernlund, J.R., Dahlin, T., 2010. Geoelectrical imaging in the interpretation
1 710 of geological conditions affecting quarry operations. Bull. Engineering Geology Environment
2
3 711 69, pp. 465–486.
- 4
5 712 41. McNeill, J.D., Bosnar, M., and Snelgrove, F.B., 1990. Resolution of an electromagnetic
6
7 713 borehole conductivity logger for geotechnical and ground water applications: Geonics
8
9 714 Technical Note TN–25, 28 pp.
- 10
11
12
13 715 42. Merriam J.B., 2007. Induced polarization and surface electrochemistry. Geophysics 72 (4),
14
15 716 pp. 157-166.
- 16
17
18 717 43. Miall, A.D., 2000. Principles of Sedimentary Basin Analysis. Third, updated and enlarged
19
20
21 718 edition. ISBN 978-3-642-08506-2. ISBN 978-3-662-03999-1 (eBook). <https://doi>
22
23 719 [10.1007/978-3-662-03999-1](https://doi.org/10.1007/978-3-662-03999-1).
- 24
25
26 720 44. Michael, H.A., Scott, K.C., Koneshloo, M., Yu, X., Khan, M.R., Li, L., 2016. Geologic
27
28 721 influence on groundwater salinity drives large seawater circulation through the continental
29
30 722 shelf. Geophysical Research Letters 43, pp. 10782–10791.
31
32 723 <https://doi.org/10.1002/2016GL070863>.
- 33
34
35
36 724 45. Ntarlagiannis, D., Williams, K.H., Slater, L., Hubbard, S., 2005a. Low-frequency electrical
37
38 725 response to microbial induced sulfide precipitation. Journal of Geophysical. Research 110.
39
40 726 G02009. <https://doi.org/10.1029/2005JG000024>.
- 41
42
43
44 727 46. Nguyen, F., Kemna, A., Antonsson, A., Engesgaard, P., Kuras, O., Ogilvy, R., Gisbert, J.,
45
46 728 Jorreto, S., and Pulido-Bosch, A., 2009. Characterization of seawater intrusion using 2D
47
48 729 electrical imaging. Near Surface Geophysics 7, No. 5–6: pp. 377–390.
- 49
50
51 730 47. Nguyen, T.T., Karl, S., Danie, U., Charles, N., Phung, V.P., Paul, L., DeMaster, D., Bui,
52
53 731 V.D., Le, D.A., Mai, D.D., 2017. Surface sediment grain-sized distribution and sediment
54
55 732 transport in the subaqueous Mekong Delta, Vietnam. Vietnam Journal of Earth Sciences
56
57 733 39(3), pp. 193-209, DOI: 10.15625/0866-7187/39/3/10266. Assessed available:
58
59 734 <https://vjs.ac.vn/index.php/jse/article/view/10266/pdf>.
- 60
61
62
63
64
65

- 735 48. Nguyen Van Vuong., 1991. The quantitative lithological method for recognition of the
1 736 unconsolidated sedimentary formation environments. *Journals of geology*, pp. 206 – 207.
2
3 737 Assessed available: http://www.idm.gov.vn/nguon_luc/Xuat_ban/1991/a20611.htm.(In
4
5 Vietnamese)
6 738
7
8 739 49. Ogilvy, A. A., and Kuzmina, E. N., 1972. Hydrogeologic and engineering-geologic
9
10 possibilities for employing the method of induced potentials: *Geophysics* 37, pp. 839–861.
11 740
12
13 741 50. Olhoeft, G. R., 1985. Low-frequency electrical properties, *Geophysics* 50, pp. 2492–2503.
14
15
16 742 51. Post, V.E.A., M. Eichholz, R. Brentführer., 2018. Groundwater management in coastal zones.
17
18 Bundesanstalt für Geowissenschaften und Rohstoffe (BGR). Hannover, Germany, 107 pp.
19
20 744 Assessed available:
21
22 [https://www.bgr.bund.de/EN/Themen/Wasser/Produkte/Downloads/groundwater_managem](https://www.bgr.bund.de/EN/Themen/Wasser/Produkte/Downloads/groundwater_management_in_coastal_zones.pdf?__blob=publicationFile&v=3)
23 745 [ent_in_coastal_zones.pdf?__blob=publicationFile&v=3](https://www.bgr.bund.de/EN/Themen/Wasser/Produkte/Downloads/groundwater_management_in_coastal_zones.pdf?__blob=publicationFile&v=3).
24
25 746
26
27 747 52. Revil, A., Coperey A., Shao, Z., Florsch, N., Fabricius, I. L., Deng, Y., Delsman, J. R., Pauw,
28
29 P. S., Karaoulis, M., De Louw, P. G. B., Van Baaren, E. S., Dabekaussen, W., Menkovic, A.,
30 748
31 and Gunnink, J. L ., 2017. Complex conductivity of soils, *Water Resource Research* 53, pp.
32 749
33 7121–7147, doi:10.1002/ 2017WR020655.
34
35 750
36
37 751 53. Revil A., 2012. Spectral induced polarization of shaly sands: Influence of the electrical double
38
39 layer. *Water Resources Research* 48(2), W02517, doi:10.1029/2011WR011260.
40 752
41
42 753 54. Revil, A., and M. Skold., 2011. Salinity dependence of spectral induced polarization in sands
43
44 and sandstones, *Geophysical Journal International* 187, pp. 813–824, doi:10.1111/j.1365-
45 754
46 246X.2011.05181. x.
47 755
48
49 756 55. Revil, A. & Florsch, N., 2010. Determination of permeability from spectral induced
50
51 polarization data in granular media, *Geophysical Journal International* 181, pp. 1480–1498,
52 757
53 doi:10.1111/j.1365-246X.2010.04573.x
54 758
55
56
57 759 56. Ronald L. Malcolm and V. C. Kennedy., 1970. Variation of Cation Exchange Capacity and
58
59 Rate with Particle Size in Stream Sediment. *Journal (Water Pollution Control Federation)*,
60 760
61
62
63
64
65

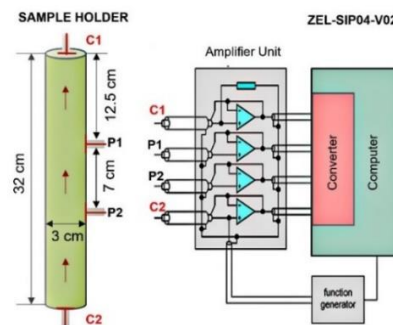
- 761 Vol. 42, No. 5, Research Supplement to: 42, 5, Part II pp. 153-160.
762 <https://www.jstor.org/stable/25036587>.
- 763 57. Saneiyani, S., Ntarlagiannis, D., Werkema, D.D., Ustra, A., 2018. Geophysical methods for
764 monitoring soil stabilization processes. *Journal of Applied Geophysics* 148, pp. 234–244.
765 <https://doi.org/10.1016/j.jappgeo.2017.12.008>.
- 766 58. Sara, J., Anders, L., Gianluca, F., and Dahlin, T., 2020. Spectral induced polarization of
767 limestones: time domain field data, frequency domain laboratory data and physicochemical
768 rock properties. *Geophysical Journal International* 220, pp. 928–950. [https://doi:](https://doi.org/10.1093/gji/ggz504)
769 [10.1093/gji/ggz504](https://doi.org/10.1093/gji/ggz504).
- 770 59. Slater, L.D., Lesmes, D., 2002. IP interpretation in environmental investigations. *Geophysics*.
771 67, pp. 77–88.
- 772 60. Slater, L., Binley, A., Daily, W., Johnson, R., and Binley, A., 2000. Cross-hole electrical
773 imaging of a controlled saline tracer injection: *Journal of Applied Geophysics* 44, pp. 85–
774 102.
- 775 61. Szalai, S., Novák, A., Szarka, L., 2009. Depth of investigation and vertical resolution of
776 surface geoelectric arrays. *Journal of Environmental and Engineering Geophysics* 14(1),
777 pp.15–23. <https://doi.org/10.2113/JEEG14.1.15>.
- 778 62. Ta T.K.O., Nguyen V.L., Kobayashi I., Tateishi M and Saito Y., 2001. Late Pleistocene-
779 Holocene stratigraphy and delta progradation, the Mekong River delta, South Vietnam.
780 *Gondwana Research* 4(4), 779 pp. Assessed available:
781 [https://www.academia.edu/56550912/Late_Pleistocene_Holocene_Stratigraphy_and_Delta_](https://www.academia.edu/56550912/Late_Pleistocene_Holocene_Stratigraphy_and_Delta_Progradation_the_Mekong_River_Delta_South_Vietnam)
782 [Progradation_the_Mekong_River_Delta_South_Vietnam](https://www.academia.edu/56550912/Late_Pleistocene_Holocene_Stratigraphy_and_Delta_Progradation_the_Mekong_River_Delta_South_Vietnam).
- 783 63. Tarasov, A., and Titov, K., 2007. Relaxation time distribution from time domain induced
784 polarization measurements, *Geophysical Journal International* 170, pp. 31–43.
- 785 64. Tassy, A., Maxwell, M., Borgomano, J., Arfib, B., Fournier, F., Gilli, E., and Guglielmi, Y.,
786 2014. Electrical resistivity tomography (ERT) of a coastal carbonate aquifer (Port-Miou, SE

- 787 France). *Environmental Earth Sciences* 71, pp. 601–608. [http://doi.10.1007/s12665-013-](http://doi.10.1007/s12665-013-2802-4)
1 788 2802-4.
2
- 3 789 65. Titov, K., Tarasov, A., Ilyin, Y., Seleznev, N., Boyd, A., 2010. Relationships between induced
4
5 790 polarization relaxation time and hydraulic properties of sandstone. *Geophysical Journal*
6
7
8 791 *International* 180, pp. 1095–1106. <https://doi.org/10.1111/j.1365-246X.2009.04465.x>.
9
- 10 792 66. Titov, K., Kemna, A., Tarasov, A., and Vereecken, H., 2004. Induced Polarization of
11
12
13 793 Unsaturated Sands Determined through Time Domain Measurements. *Vadose Zone Journal*
14
15 794 Vol 3, pp. 1160–1168.
16
- 17 795 67. Tran, N., Nguyen-Thanh, L., Dinh, X.T., Pham, N.H.V., Nguyen, H.S., Tran, T.T.N., 2007.
18
19
20 796 Quaternary sedimentary cycles in relation to sea level change in Vietnam. *VNU Journal of*
21
22
23 797 *Science, Earth Sciences* 23, pp. 235-243.
24
- 25 798 68. Vacquier, V., Holmes, R., Kintzinger, P. R., and Lavergne, M., 1957. Prospecting for ground
26
27
28 799 water by induced electrical polarization: *Geophysics* 22, pp. 660–687.
29
- 30 800 69. Vandenbohede, A., Lebbe, L., Gysens, S. & De Wolf, P., 2008. Infiltration of salt water in
31
32
33 801 artificial sea inlets in the Belgian dune area. In: *Proceedings of the 1st SWIM-SWICA (19th*
34
35 802 *Salt Intrusion Meeting – 3 rd Salt Water Intrusion in Coastal Aquifers)*, pp. 239- 245.
36
- 37 803 70. Vaudelet, P., Revil, A., Schmutz, M., Franceschi, M. and Bégassat, P., 2011. Induced
38
39
40 804 polarization signatures of cations exhibiting differential sorption behaviors in saturated sands.
41
42 805 *Water Resources Research* 47(2), W02526, doi:10.1029/2010WR009310.
43
- 44 806 71. Vinegar, H.J. and Waxman, M.H., 1984. Induced Polarization of Shaly Sands. *Geophysics* 49,
45
46
47 807 pp. 1267-1287. <http://dx.doi.org/10.1190/1.1441755>.
48
- 49 808 72. von Bülow, R., Klitzsch, N., and Wellmann, F., 2021. Strategies to overcome near surface
50
51
52 809 disturbances while inverting time-lapse surface ERT data. *Journal of Applied Geophysics*
53
54 810 195,104463 pp. <https://doi.org/10.1016/j.jappgeo.2021.104463>.
55
56
- 57 811 73. Waxman, W.H., Smits L.J.M., 1968. Electrical conductivities in oil-bearing sands. *Social*
58
59
60 812 *Petroleum Engineering Journal* 8, pp. 107-122.
61
62
63
64
65

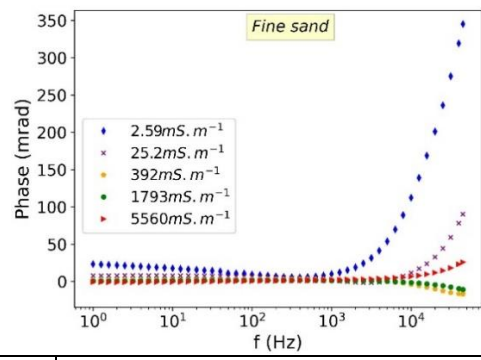
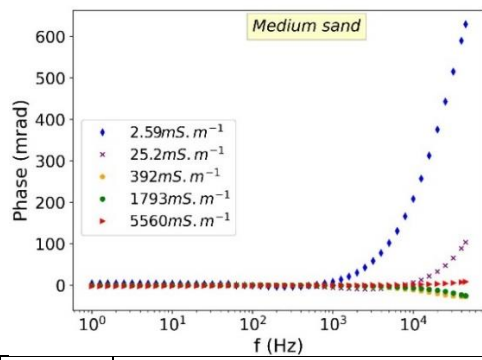
- 813 74. Weigand, M., and Kemna, A., 2016. Relationship between Cole-Cole model parameters and
 1 814 spectral decomposition parameters derived from SIP data. *Geophysical Journal International*
 2
 3 815 205, pp. 1414–1419. [https://doi: 10.1093/gji/ggw099](https://doi.org/10.1093/gji/ggw099).
 4
 5
 6 816 75. Wentworth, C. K., 1922. A scale of grade and class terms for clastic sediments. *Journal of*
 7
 8 817 *Geology*, vol. 30, 377 pp.
 9
 10
 11 818 76. Zimmermann, E., Kemna, A., Berwix, J., Glaas, W., Münch, H.M., Huisman, J.A., 2008. A
 12
 13 819 high-accuracy impedance spectrometer for measuring sediments with low polarizability.
 14
 15 820 *Measurement Science and Technology* 19, 105603 pp. doi:10.1088/0957-0233/19/10/105603.
 16
 17
 18
 19 821 77. Zarif, F., Kessouri, P., and Slater, L., 2017. Recommendations for field-scale induced
 20
 21 822 polarization (IP) data acquisition and interpretation. *Journal of Environmental and*
 22
 23 823 *Engineering Geophysics*. Volume 22, Issue 4, pp. 395–410. [http://doi.10.2113/JEEG22.4.395](http://doi.org/10.2113/JEEG22.4.395).
 24
 25
 26
 27 824 78. Zimmermann, E., Huisman, J.A., Kemna, A., Berwix, J., Glaas, W., Meier, H., Wolters, B.,
 28
 29 825 Esser, O., 2010. Advanced electrical impedance tomography system with high phase
 30
 31 826 accuracy. Presented at the 6th World Congress on Industrial Process Tomography, pp. 583–
 32
 33 827 591.
 34
 35
 36
 37

APPENDIX

A. SIP measurements (Zimmermann et al., 2008) and our cylinder-shaped sample holder.



830 **B.:** Normalized chargeability of the clay-bearing groups is calculated in the frequency domain. Graphs
 831 refer to phase shift spectra through the five salinity solutions in medium and fine sand categories are nearly
 832 flat at the low-frequency range.



Clay content (%)	Fz	Quadrature conductivity (mS.m ⁻¹)					Normalized chargeability (mS.m ⁻¹)				
		2.59 mS.m ⁻¹	25.2 mS.m ⁻¹	392 mS.m ⁻¹	1793 mS.m ⁻¹	5560 mS.m ⁻¹	2.59 mS.m ⁻¹	25.2 mS.m ⁻¹	392 mS.m ⁻¹	1793 mS.m ⁻¹	5560 mS.m ⁻¹
17	1.00E+03	0.6793	0.6642	1.2029	1.6826	2.1245	3.4	3.3	6.0	8.4	10.6
	1.00E+02	0.3507	0.3548	0.6957	0.9954	1.2828	1.8	1.8	3.5	5.0	6.4
	1.00E+01	0.1933	0.1727	0.4395	0.5580	0.7482	1.0	0.9	2.2	2.8	3.7
	1.00E+00	0.1082	0.1009	0.2721	0.1836	0.1856	0.5	0.5	1.4	0.9	0.9
25	1.00E+03	1.5489	1.4770	1.5673	1.5311	1.3702	7.7	7.4	7.8	7.7	6.9
	1.00E+02	0.8694	0.8514	0.9355	0.9366	0.8488	4.3	4.3	4.7	4.7	4.2
	1.00E+01	0.5385	0.4739	0.5398	0.4349	0.1389	2.7	2.4	2.7	2.2	0.7
	1.00E+00	0.3140	0.2630	0.2958	0.2167	0.2343	1.6	1.3	1.5	1.1	1.2
30	1.00E+03	1.8086	1.8580	1.7468	1.8274	2.0637	9.0	9.3	8.7	9.1	10.3
	1.00E+02	1.0870	1.1444	1.0723	1.1911	1.1563	5.4	5.7	5.4	6.0	5.8
	1.00E+01	0.6172	0.6503	0.5907	0.5868	0.3364	3.1	3.3	3.0	2.9	1.7
	1.00E+00	0.3013	0.3365	0.2672	0.2591	0.2106	1.5	1.7	1.3	1.3	1.1
35	1.00E+03	1.2522	1.1349	1.7622	2.0788	2.9548	6.3	5.7	8.8	10.4	14.8
	1.00E+02	0.6195	0.5688	0.8976	1.0685	1.5365	3.1	2.8	4.5	5.3	7.7
	1.00E+01	0.3324	0.3176	0.4127	0.3596	0.4324	1.7	1.6	2.1	1.8	2.2
	1.00E+00	0.1733	0.1723	0.1743	0.0488	0.3175	0.9	0.9	0.9	0.2	1.6

833 C. Total dissolved content (TDS) and electrical conductivity in the drilled boreholes of the Luy River
 834 Catchment in both dry and rainy seasons during two years.

Boreholes			2020		2021			
No	Name	Depth (m)	Rainy season		Dry season		Rainy season	
			TDS (mg/L)	EC (mS/m at 25°C)	TDS (mg/L)	EC (mS/m at 25°C)	TDS (mg/L)	EC (mS/m at 25°C)
1	LK01-BT	32	11146	1715	43200	6646	6579	1012
2	LK02-BT	12	1664	256	1743	268	824	127
3	LK03-BT	17	8257	1270	11800	1816	6318	972
4	LK04-BT	8	941	145	2858	440	1251	193
5	LK07-BT	13.5	14212	2187	31620	4865	20610	3171
6	LK08*-BT	4.5	631	97	1315	203	471	73
7	LK09-BT	20.5	893	137	1435	221	694	107
8	LK10-BT	9	496	76	-	-	607	93
9	LK11-BT	13.5	512	79	570	88	303	47
10	LK12-BT	8	544	84	598	92	335	52
11	LK13-BT	23	880	135	1449	223	880	135
12	LK14-BT	16	1049	162	2010	309	1119	172

13	LK15-BT	13	535	82	362	56	132	20
14	LK16-BT	9	377	58	286	44	115	18
15	LK17-BT	21.5	2702	416	5645	869	1564	241
16	LK18-BT	13	579	89	1522	234	1540	237
17	LK19-BT	13.5	1277	197	1522	234	1102	170
18	LK20-BT	9	397	61	1184	183	139	21

835

1
2
3
4
5
6
7
8
9
10
11
12
13
14
15
16
17
18
19
20
21
22
23
24
25
26
27
28
29
30
31
32
33
34
35
36
37
38
39
40
41
42
43
44
45
46
47
48
49
50
51
52
53
54
55
56
57
58
59
60
61
62
63
64
65